Journal of Ship Research, Vol. 57, No. 4, December 2013, pp. 241–261
http://dx.doi.org/10.5957/JOSR.57.4.130031

Parametric Generation of Planing Hulls with NURBS Surfaces

Francisco L. Pérez-Arribas and **Ernö Péter-Cosma**

Naval Architecture School of Madrid, Universidad Politécnica de Madrid (UPM), Madrid, Spain

This article presents a mathematical method for producing hard-chine ship hulls based on a set of numerical parameters that are directly related to the geometric features of the hull and uniquely define a hull form for this type of ship. The term planing hull is used generically to describe the majority of hard-chine boats being built today. This article is focused on unstepped, single-chine hulls. B-spline curves and surfaces were combined with constraints on the significant ship curves to produce the final hull design. The hard-chine hull geometry was modeled by decomposing the surface geometry into boundary curves, which were defined by design constraints or parameters. In planing hull design, these control curves are the center, chine, and sheer lines as well as their geometric features including position, slope, and, in the case of the chine, enclosed area and centroid. These geometric parameters have physical, hydrodynamic, and stability implications from the design point of view. The proposed method uses two-dimensional orthogonal projections of the control curves and then produces three-dimensional (3-D) definitions using B-spline fitting of the 3-D data points. The fitting considers maximum deviation from the curve to the data points and is based on an original selection of the parameterization. A net of B-spline curves (stations) is then created to match the previously defined 3-D boundaries. A final set of lofting surfaces of the previous B-spline curves produces the hull surface.

Keywords: planing hulls; hard-chine boats; B-splines; parametric design; ship surface design

1. Introduction

Defining a ship hull is one of the most limiting processes in initial ship design. A hull form is usually designed by modifying an existing hull (template or parent hull), which can include direct manipulation of the surface control vertices when B-spline or NURBS (nonuniform rational B-spline) surfaces are used. Although this has become a standard practice and produces good results, it necessitates much manual work because the designer must manipulate individual control vertices. Furthermore, this process does not allow for rapid creation or modification of the hull surface in the initial phases of the ship design process. Finally, using this method, important characteristics of the ship hull cannot be determined until a later calculation is made, which necessitates a trial and error procedure. Thus, a hull form should be generated as early as possible to provide demanded design calculations that are important for subsequent design stages such as stability, hydrostatics, lift, drag, and layout drawings.

The parametric generation of a ship hull can ensure that a set of design parameters is met and preserved when creating a complete hull form and that the design algorithm generates an appropriate hull that is constrained by the design parameters without further human interaction. However, a parametric method is limited to the range of hulls that can be generated. In this particular method, these fixed formulations allow enough flexibility in the number of hull shapes that can be generated for a planing hull. Specifically, semidisplacement and recreational planing crafts, trawler yachts, and patrol boats can be formulated, but stepped, multichine, and multihull crafts cannot. Computational optimization techniques based on computational fluid dynamics can be used with systematic constraint definitions of a ship hull to produce faster, more comfortable and safer planing hulls. These optimization methods require complete geometric details of the design and correct management of hull information so that one can understand the relationship between the optimization method and the constrained design of the hull.

Manuscript received at SNAME headquarters July 12, 2011; revised manuscript received October 2, 2013.

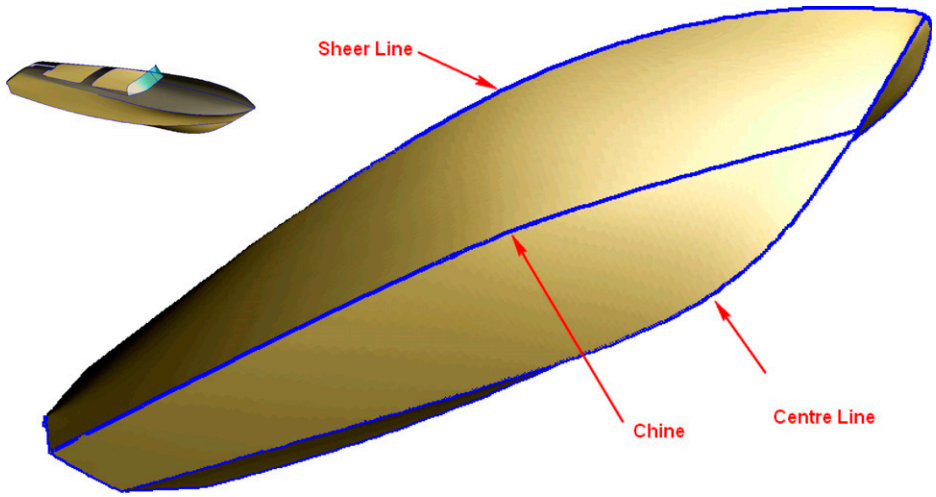

Fig. 1 Geometry of a planing hull

This article presents a parametric design method for defining planing hulls with the previously mentioned range of applicability. Practical examples will be used to show how the proposed method affords reliable hull design solutions. Figure 1 presents an example of a hull that can be automatically defined with the presented method and shows the boundary curves that define that hull.

This article is organized as follows. First, Section 2 provides a background on parametric design. Then, Section 3 describes the proposed method beginning with the conception of the boundary curves shown in Fig. 1 based on their orthogonal two-dimensional (2-D) projections. A B-spline scheme for these curves is adopted, and linear or nonlinear problems are solved to obtain a constrained definition that agrees with the geometric design parameters selected by the designer. A direct three-dimensional (3-D) approach to boundary curve definition would require a great number of parameters to uniquely define the curves, and some of these parameters would be purely mathematical such as curvatures or derivatives that are either difficult to define in the initial design stage or are not of practical use for a naval architect. For this reason, an initial 2-D approach was used.

The description of the method continues with the definition of the 3-D boundary lines in Section 3.6 using constrained B-spline fitting of the points obtained from 2-D curves. This fitting uses a parameterization based on the distance from the data points to the B-spline. This is useful for manufacturing purposes because it enables an assessment of the maximum or average deviations from the original curves.

A net of B-spline curves (stations) is then created in Section 3.7 that match the previously defined 3-D boundaries. A final set of lofting surfaces from the previous B-spline curves produces the hull surface.

Finally, Section 4 presents two hulls designed with the presented methodology to demonstrate the validity of the proposed method. Section 5 presents the major conclusions of the article.

2. Background

Parametric design methodologies can be traced back to Kuiper (1970), who generated hull shapes in the 1970s using conformal mapping techniques from hull parameters rather than from offset hull data points. Kuiper generated hulls by constructing different waterline polynomials according to coefficients controlled by draught functions. The hull representation techniques of that time did not allow the development of hull shapes in a convenient and accurate way.

Reed and Nowacki (1974) developed a compromise between polynomials and conformal mapping techniques; namely, polynomials were used to represent the hull above the waterline, and conformal mapping techniques were used for the underwater part of the ship. B-splines and NURBS functions were used by Creutz and Schubert (1978) for ship hull design. They developed a procedure to generate B-spline curves from form parameters. These early studies demonstrated how NURBS and B-splines could adequately represent the geometry of a ship hull.

Keane (1988) developed simple hulls using constrained generation techniques based on conformal mapping and studied the influence of certain parameters on ship stability. This is one of the first optimization procedures to be based on parameter variation. Yilmatz and Kukner (1999) determined hull stations parametrically by applying a regression technique to a large database of hulls. This method can only be used for certain fishing vessels because those ships were used to construct the database. Mancuso (2006) used parametric methods to define sailing ship hulls and the authors of the present article developed a method for round bilge hulls (Pérez et al. 2008).

Different authors such as Bole (2002), Kim (2004), and Nam and Parsons (2006) researched this topic by subdividing the ship hull into multiple domains such as the entrance, flat bottom, and flat side. The proposed method will subdivide planing hulls into one domain below the chine line and one above the chine line. In the case that a spray rail is present, a third domain will be implemented.

Based on the previous references, it can be observed that the use of parametric techniques in ship design is not unusual in the literature. However, the applicability of these techniques to hard-chine planing hulls is quite limited. We found only one notable reference, Calkins et al. (2001), that defined a planing hull using a parametric methodology, but it did not include B-spline modeling, which is a standard in naval architecture; rather, it

covered the hull shape with straight stations, which is unrealistic most of the time.

The use of parameters to study the hydrodynamic properties of hard-chine hulls is quite common, like in the significant papers in this field written by Clement and Blount (1963), Savitsky (1964), Savitsky and Brown (1976), and Blount and Codega (1992). These papers motivated the present work. Commercial hull design software packages now include modules for the basic, constrained generation of ship hulls, demonstrating that designers have a clear need for such a technique.

These commercial software modules were reviewed by Bole (2002). Some of the software packages use nonintuitive parameters such as curvatures, derivatives, or numerical weights. Other packages are limited on the other end, producing very simple hulls based only on primary dimensions that do not cover specific parameters for a planing hull such as the dead-rise angle, enclosed chine area, or stem angles.

The transformation of a parent hull is limited as a result of the numerical techniques that are used. These methods (Lackenby transformations) are based on relocating and scaling hull sections while maintaining the desired dimensions in a trial-and-error manner until a selected displacement and longitudinal center of buoyancy are reached.

The main reason that these methods are not appropriate for planing hulls is that a planing hull is not a volumetric ship; this produces a completely different set of initial parameters. Displacement ship design starts with the definition of its sectional area curve and waterplane curve based on their associated parameters (e.g., block coefficient and centroid, waterplane area coefficient). On the other hand, a designer of planing boats typically considers concepts such as dead-rise, chine development, and warp, which are used by the routines designed for planing boats such as dynamic equilibrium and ride comfort analysis or which are evaluated according to the designer's own experience from previous designs.

A review of the literature suggested that a constrained definition of a ship hull can be successfully made by directly generating the hull surface from numerical parameters, as described in the present article, or by altering the shape of a given hull surface (template) to match specified parameters. This last technique is commonly used in numerical optimization papers for planing hulls such as those by Ayob et al. (2009, 2010). In these papers, automatic surface information retrieval from offset data was performed using B-splines, and the resulting ship geometry was used as a template for geometric variation through parametric transformation.

Using hull surface template modification techniques, the hull can be created using direct vertex modification by the designer. This group of methods is more flexible regarding the types of hulls that can be defined, but the templates cannot be defined or altered. Furthermore, templates can be difficult to manage for a nonadvanced user and demand a lot of manual work. Constrained generation tools build the hull surface representation from relatively few parameters, and this information is used to determine the shapes and volumetric properties of the hull.

3. Description of the method

The geometry of a single chine unstepped hull can be defined by the lines shown in Fig. 1. This type of hull has a flat transom stern and can be modeled by decomposing the surface into boundaries or control curves that will be constrained by the design parameters. These numerical parameters include position and slope. In the case of the chine, which is the most significant curve of a planing hull design, the enclosed area (Ac) and centroid (X_C) are also included in the numerical parameters. The boundary curves are the keel or centerline (CL), the chine line, and the sheer line. The objective of the presented method is to create B-spline surfaces to represent a ship hull based on the constraints displayed in Table 1 with the graphical meaning depicted in Fig. 2.

The parameters in Table 1 have the graphical meaning depicted in Fig. 2, where the vectors indicate the angle between the X-axis and the arrow line.

Table 1 Parameters of the method (see also Fig. 2)

Name	Description	Location
	Length	
Ls	Abscissa of the forward-most point of the sheer line	Center, sheer
L0	Abscissa where the forefoot is tangent to the keel line	Center
Lx	Abscissa of the sheer's maximum breadth	Sheer (plan)
Lc	Abscissa of the forward-most point of the chine	Center, chine
Xc	Abscissa of the centroid of Ac	Chine (plan)
X_{C1}	Abscissa of an intermediate point of the chine	Chine (profile)
	Width	
Bs	Sheer's half-breadth at the transom	Sheer (plan)
Bx	Ordinate of the sheer's maximum half-breadth	Sheer (plan)
Bc	Chine's half-breadth at the transom	Chine (plan)
Sp	Width of the spray rail at the transom	Three-dimensional
	Height	
Hs	Height of the foremost point of the sheer	Center, sheer (profile)
Hc	Height of the foremost point of the chine	Center, chine (profile)
r	Rocker at the transom	Center
hs	Sheer's height at the transom	Sheer (profile)
hc	Chine's height at the transom	Chine (profile)
Z_{C1}	Height of X_{C1}, normally the draft of the ship	Chine (profile)
	Angles	
α_K	Angle at the stem	Center
α_S	Angle at the foremost point of the sheer in plan view	Sheer (plan)
β's	Angle at the transom of the sheer in lateral view	Sheer (profile)
α's	Angle at the foremost point of the sheer in lateral view	Sheer (profile)
α_C	Angle at the foremost point of the chine in plan view	Chine (plan)
β_C	Angle at the transom point of the chine in plan view	Chine (plan)
α'_C	Chine's angle at the foremost point in profile view	Chine (profile)
β'_C	Chine's angle at the transom point in profile view	Chine (profile)
	Areas	
$2 \cdot Ac$	Enclosed area between the chine and the X-axis in plan view	Chine (plan)

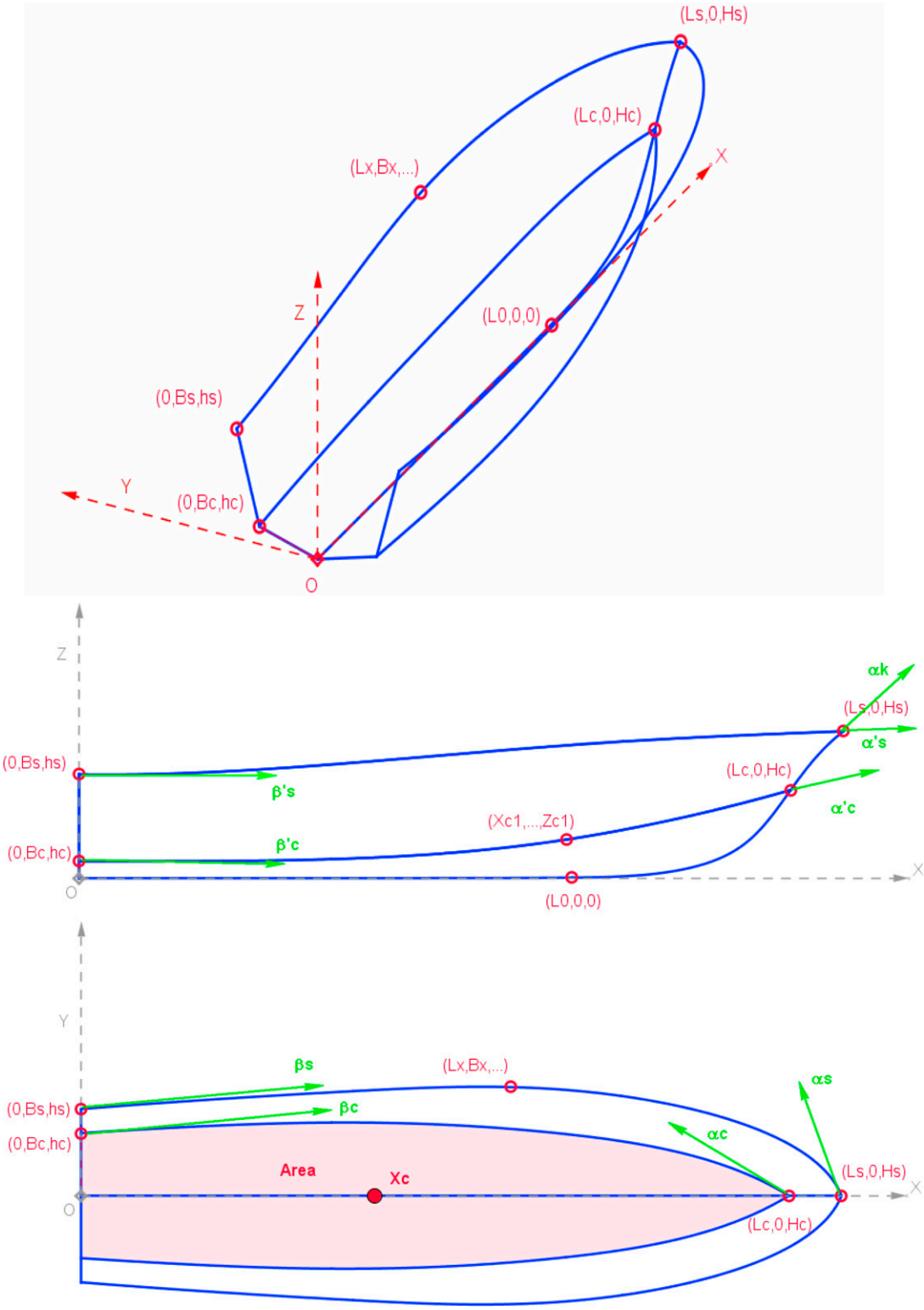

Fig. 2 Graphical representation of the parameters

The selected parameters used to define these curves have meaning for the ship designer and can be related to further aspects of ship design. The curve definition has been simplified by considering that the hull has a flat vertical transom and that the aftermost point of all the curves has a zero abscissa as in Fig. 2. In the case of a nonvertical transom, the definition can be easily reconfigured to consider a nonzero abscissa for the aforementioned points, which will be a function of the transom angle.

A very important design feature, the transom dead-rise angle, Ω, is derived from hr, hc, and Bc, $\Omega = \text{Arctan}(\frac{hc - hr}{Bc}) \cdot \frac{180}{\pi}$ in degrees. The overall maximum dimensions of the length and breadth of the hull are Ls and $2 \cdot Bx$, respectively. The method allows the definition of a spray rail of a given width, Sp, along the chine, as will be explained in Section 3.6.

The method splits up the stations into two different domains: below and above the chine. The method controls the concavity/convexity of these curves using a parameter that controls the maximum deviation of every station piece from a straight segment, as detailed in Section 3.7.

To introduce the notation for the article, a brief review of B-splines follows. A B-spline curve is formed by several pieces of polynomial curves, called Bézier pieces, and the whole curve is C^2 (common curvature or second derivatives) at the junctions in the case of cubic B-splines. The curve is defined with a polygon, called the control polygon, and with an interpolation algorithm that allows its construction to relate the curve to the control polygon. The interpolation steps are encoded in a family of piecewise polynomial functions, $B_j^n(u)$, called B-spline functions of the n^{th} degree and are calculated using De Boor's algorithm (Farin 2001). Cubic B-splines are the most widely used curves in ship design and the ones that generally fit better the traditional loftsman's splines.

A B-spline curve, $\boldsymbol{s(u)}$ in equation (1), is a linear combination of basis functions and $m + 1$ control points, $\boldsymbol{P_j}$, as coefficients. Therefore, B-spline curves are parametric, $x = X(u)$, $y = Y(u)$, $z = Z(u)$, where the parameter u is considered inside [0,1] in this article. In the 2-D plane, $\boldsymbol{P_j} = (Xj, Yj)$, $j = 0, \ldots, m$, generate a B-spline $\boldsymbol{s(u)}$ of the n^{th} degree,

$$s(u) = \sum_{j=0}^{m} P_j \cdot B_j^n(u) = (X(u), Y(u)) = \sum_{j=0}^{m} \left(X_j \cdot B_j^n(u), Y_j \cdot B_j^n(u) \right) \quad (1)$$

where the basis functions are obtained with the De Boor's algorithm of equation (2)

$$B_j^0(u) = \begin{cases} 1 & u \in [u_{j-1}, u_j) \\ 0 & u \notin [u_{j-1}, u_j) \end{cases} \quad B_j^n(u) = \frac{u - u_{j-1}}{u_{j+n-1} - u_{j-1}} \cdot B_j^{n-1}(u) + \frac{u_{j+n} - u}{u_{j+n} - u_j} \cdot B_{j+1}^{n-1}(u) \quad (2)$$

The basis functions, $B_j^n(u)$, depend on the knot vector, u_j. In this work, the knot vector has been selected to be uniform with a multiplicity equal to the order of the curve at its ends, where the order is defined as the degree + 1. In this manner, the B-spline interpolates the ends of its control polygon at $u = 0$ and $u = 1$, and it is tangent at its ends to the first and last segment of its control polygon. This last property simplifies the mathematical definition of the curves used in the method. Notice that the derivative, $\boldsymbol{s'(u)}$, of a B-spline is a linear combination of the derivatives of the basis functions:

$$s'(u) = \sum_{j=0}^{m} P_j \cdot B_j'^n(u) = (X(u), Y(u)) = \sum_{j=0}^{m} \left(X_j \cdot B_j'^n(u), Y_j \cdot B_j'^n(u) \right) \quad (3)$$

Table 2 Basis and derivative functions of the B-splines for the presented method

j	B_j^3	B'^3_j	B_j^2	B'^2_j
0	1 to 3·u + 3·u^2-u^3	−3 + 6·u-3·u^2	(1-u)^2	−2·(1-u)
1	3·u-6·u^2 + 3·u^3	3 to 12·u + 9·u^2	2·u·(1-u)	2 to 4·u
2	3·u^2-3·u^3	6·u-9·u^2	u^2	2u
3	u^3	3·u^2	0	0

One form of the basis functions of equation (2) and their derivatives for cubic and quadratic B-splines of 4 and 3 control points and a uniform knot vector are shown in Table 2. The curves of the following sections use these functions in their definitions.

When the number of control points ($m + 1$) is equal to the order of the curve ($n + 1$), the B-spline curve is formed with only one piece and can be called a Bézier curve of n^{th} degree. In this work, all the curves will be referred to as B-splines for the sake of clarity. A variable presented in bold letters indicates that this element is formed from several components such as points, vectors, or B-spline curves that have an X, Y, and Z component.

Background figures corresponding to real ship designs have been used to show how the B-spline curves of the method produce realistic results in the figures of the following sections.

3.1. Definition of the centerline

The center or keel line is usually without appendages or a skeg and runs in a straight line forward to the transom (**O**). This line curves up toward the stem at the start of the forefoot $\mathbf{K_0}(L_0, 0)$ and arrives at the stem at $\mathbf{K_2}(L_s, H_s)$ with a given angle (α_K). The CL contains the chine's fore end $\mathbf{K_1}(Lc, Hc)$, see Fig. 3.

With these assessments, the geometric problem consists of finding a B-spline starting at $\mathbf{K_0}$ with a zero angle and arriving at $\mathbf{K_2}$ with an angle α_K and then interpolating a point $\mathbf{K_1}$. This can be obtained with a cubic B-spline of 4 control points with the form of:

$$c(u) = B_0^3 \cdot K_0 + B_1^3 \cdot P_1 + B_2^3 \cdot P_2 + B_3^3 \cdot K_2$$

The unknown values will be the coordinates of $\mathbf{P_1}(XP_1, ZP_1)$ and $\mathbf{P_2}(XP_2, ZP_2)$ because the curve will contain the end points $\mathbf{K_0}$ and $\mathbf{K_2}$, and they will be obtained after imposing the constraints. The first two constraints are related to the tangent angles at the ends of the curve: $c_z'(0) = 0$ and $c'_z(1) = \text{tg}(\alpha_K)$. The third constraint indicates that the curve interpolates the point $\mathbf{K_1}$ for a certain parameter u^*: $\mathbf{c}(u^*) = \mathbf{K_1}$. The value of this parameter is selected according to the centripetal parameterization, which depends on both the Euclidean distance (Dist[ ]) of $\mathbf{K_1}$ to the ends of the curve and an exponent k:

$$u^* = \frac{\text{Dist}(K_0, K_1)^k}{\text{Dist}(K_0, K_1)^k + \text{Dist}(K_1, K_2)^k} \quad (4)$$

The value $k = 1$ produces a chord-length parameterization and gives good results for the CL. The constraints $c'(0) = 0$, $c'(1) = \mathrm{tg}(\alpha_K)$ and $\mathbf{c}(u^*) = \mathbf{K_1}$ produce a linear system of four equations with the following matrix form:

$$\begin{bmatrix} 0 & 1 & 0 & 0 \\ 0 & 0 & -\mathrm{tg}(\alpha_K) & 1 \\ B_1^3(u^*) & 0 & B_2^3(u^*) & 0 \\ 0 & B_1^3(u^*) & 0 & B_2^3(u^*) \end{bmatrix} \cdot \begin{bmatrix} \mathrm{XP}_1 \\ \mathrm{ZP}_1 \\ \mathrm{XP}_2 \\ \mathrm{ZP}_2 \end{bmatrix} = \begin{bmatrix} 0 \\ \mathrm{Hs} - \mathrm{tg}(\alpha_K) \cdot \mathrm{Ls} \\ \mathrm{Lc} - B_0^3(u^*) \cdot L_0 - B_3^3(u^*) \cdot \mathrm{Ls} \\ \mathrm{Hc} - B_3^3(u^*) \cdot \mathrm{Hs} \end{bmatrix} \tag{5}$$

The solution of this system of equations, which can be obtained with, for example, the Gauss-Jordan method, produces the final form of the CL. Notice how a plumb bow (Fig. 4) can be obtained, thereby reducing the forefoot radius by increasing the value of α_K and moving $\mathbf{K_2}$ backward closer to $\mathbf{K_1}$.

The shape of the forefoot can be altered while maintaining the rest of the parameters by considering different values for k in equation (4) as depicted in Fig. 5. This can be used to reduce or to increase the dead-rise angle of the forefoot sections.

Some designs may include a certain amount of rocker hr in the after-body or even some hook (negative hr), but the latter is not common in contemporary designs. This means that the CL does not run straight from the transom and that the part of the CL abaft of $\mathbf{K_0}$ has to be modeled in a different way. Realistic results can be obtained with a second-degree B-spline, $n = 2$ in equation (1), which is constructed as depicted in Fig. 6 with only three control points: $\mathbf{R_0}(0,hr)$, $\mathbf{P'_1}$ and $\mathbf{K_0}$, where $\mathbf{P'_1}$ is the symmetric point of $\mathbf{P_1}$ with respect to $\mathbf{K_0}$. This ensures that the aft part of the CL and the fore part, calculated in equation (5), are of C^1 class continuity at their joint point $\mathbf{K_0}$.

The use of different pieces to define a curve is not a problem for the proposed method and increases its flexibility because the curves can be converted into a single B-spline by considering different points on both curves. This will be explained in Section 3.6. This technique is also used to produce the 3-D curves of the chine and sheer lines from their 2-D orthogonal projections.

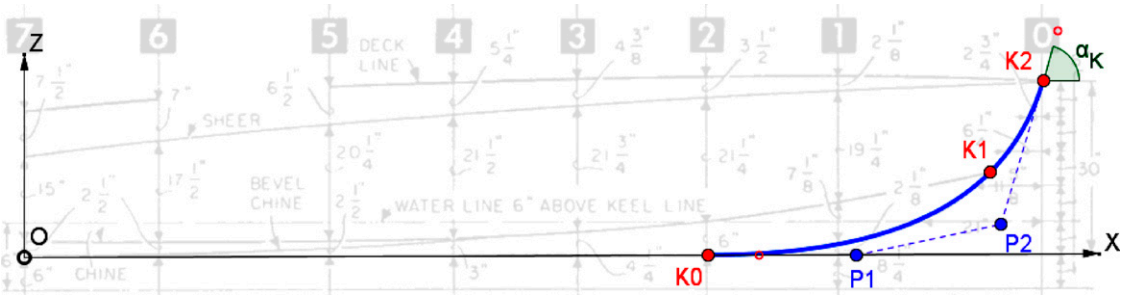

Fig. 3 Centerline definition

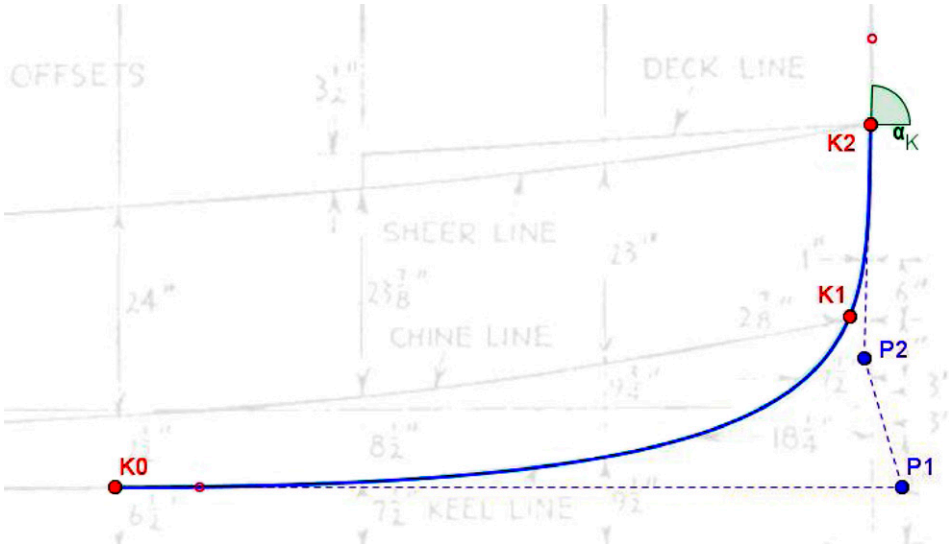

Fig. 4 Plumb bow

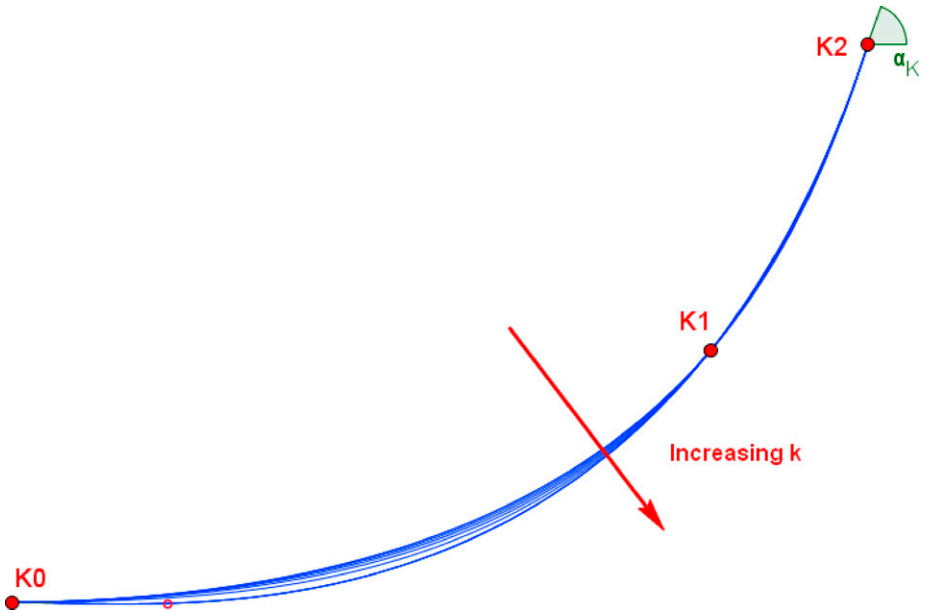

Fig. 5 Changing the forefoot by altering the parameterization

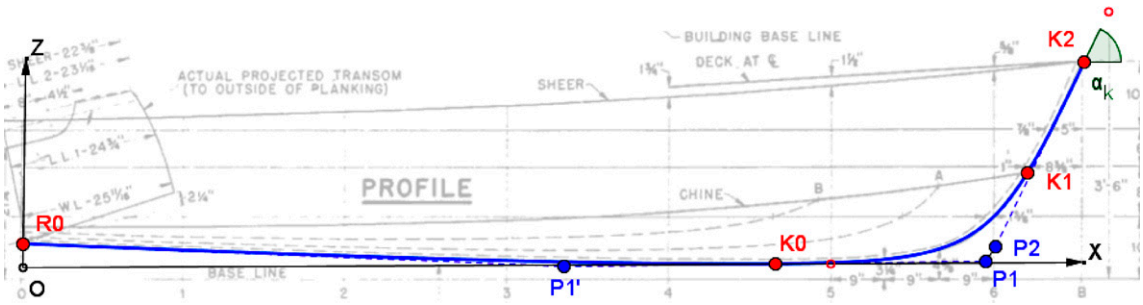

Fig. 6 Rocker in the after-body

The forefoot contour is related to the directional stability in smooth and cross seas; cross seas tend to throw the bow around. A deep forefoot with a high value of α_K produces a narrow bow and increases the dead-rise angle of the bow sections.

Styling is also a variable to be considered. There is a trend toward the use of plumb bows in new designs, especially in Europe, although it is not recommended from a hydrodynamic point of view for a planing boat.

A clipper bow that has an "S" shape above the waterline can be achieved by reducing α_K. This bow works well with a short bowsprit or anchor handling platform.

The use of a rocker is common in semidisplacement hulls designed to go more through the water than planing on top. This is because the aft buttocks are not straight. The use of a hook is not common today, and a better effect can be obtained with the use of adjustable trim tabs.

3.2. Definition of the sheer line in the plan view

In a plan view, the sheer line runs from the transom toward the stem and may have a maximum if the breadth at the transom is narrower than the maximum breadth or the maximum breadth is constant aftward, which is a common design trend. In the first case (Fig. 7), the sheer line starts at the transom, at a point $\mathbf{S_0}(0,\ Bs)$, has a maximum at $\mathbf{S_X}(Lx,\ Bx)$, and arrives at the point $\mathbf{S_2}(Ls,\ 0)$ with a given angle α_S.

The restraints of this line, $\mathbf{sp}(u)$, will be $\mathbf{s_p}(0) = \mathbf{S_0}$, $\mathbf{s_p}^{(1)} = \mathbf{S_2}$, and $\mathbf{s_p}(u^*) = \mathbf{S_x}$, together with $s'_{py}(u^*) = 0$ and $s'_p(1) = \mathrm{tg}(\alpha_S)$. Notice that the tangent angle at the transom is not imposed. These requirements are achieved with a cubic B-spline with four control points of the form:

$$s_p(u) = B_0^3 \cdot S_0 + B_1^3 \cdot P_1 + B_2^3 \cdot P_2 + B_3^3 \cdot S_2$$

The unknown values are the coordinates of $\mathbf{P_1}(XP_1,\ YP_1)$ and $\mathbf{P_2}(XP_2,YP_2)$ because the curve will contain the end points $\mathbf{S_0}$ and $\mathbf{S_2}$. These values will be obtained after imposing the constraints.

The parameter u^* is selected in the same manner as the CL, equation (4), with the chord length parameterization. The constraints $\mathbf{s_p}(0) = \mathbf{S_0}$, $\mathbf{s_p}(1) = \mathbf{S_2}$, and $\mathbf{s_p}(u^*) = \mathbf{S_X}$ together with

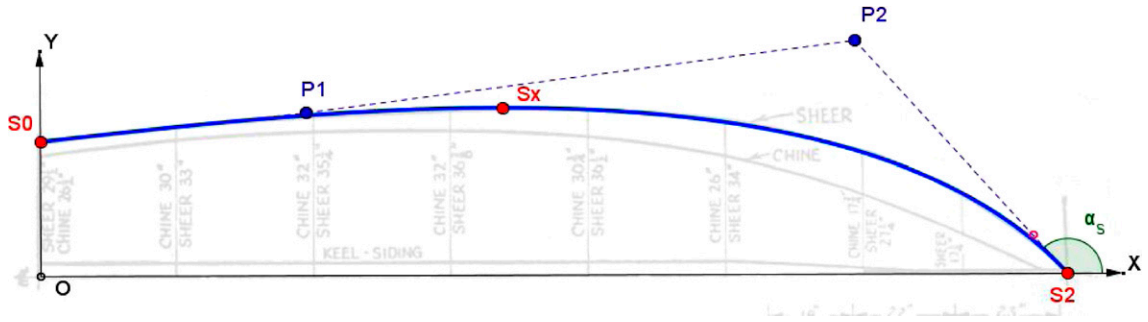

Fig. 7 Sheer line definition in plan view

$s'_{py}(u^*) = 0$ and $s'_p(1) = \mathrm{tg}(\alpha_S)$ produce a linear system of four equations with the following matrix form:

$$\begin{bmatrix} 0 & B'^3_1(u^*) & 0 & B'^3_2(u^*) \\ 0 & 0 & -\mathrm{tg}(\alpha_S) & 1 \\ B^3_1(u^*) & 0 & B^3_2(u^*) & 0 \\ 0 & B^3_1(u^*) & 0 & B^3_2(u^*) \end{bmatrix} \cdot \begin{bmatrix} \mathrm{XP}_1 \\ \mathrm{YP}_1 \\ \mathrm{XP}_2 \\ \mathrm{YP}_2 \end{bmatrix} = \begin{bmatrix} -B'_1 3(u^*) \cdot \mathrm{Bs} \\ -\mathrm{tg}(\alpha_S) \cdot \mathrm{Ls} \\ \mathrm{Lx} - B^3_3(u^*) \cdot \mathrm{Ls} \\ \mathrm{Bx} - B_0(u^*) \cdot \mathrm{Bs} \end{bmatrix} \tag{6}$$

where B^3_j and B'^3_j are obtained from Table 2 and u^* is calculated following equation (4) particularized for $\mathbf{S_0}$, $\mathbf{S_X}$ and $\mathbf{S_2}$. The solution of this system produces the control points $\mathbf{P_1}$ and $\mathbf{P_2}$, and the plan view of the sheer line is completely defined. If the sheer maintains its maximum breadth aft, then equation (6) is still valid without considering $\mathbf{S_0}$ at the transom as long as it is close enough to $\mathbf{S_x}$, as depicted in Fig. 8.

In this case, the curve is correctly defined between $\mathbf{S_X}$ ($u = u^*$) and $\mathbf{S_2}$ ($u = 1$). If $\mathbf{S_0}$ is placed at the transom, as in Fig. 9, then equation (6) produces results that are mathematically correct but are not realistic for the part of the curve between $\mathbf{S_0}$ ($u = 0$) and $\mathbf{S_X}$ ($u = u^*$). This is because $n + 1$ aligned control points are needed to define a straight portion of an n^{th} degree B-spline, which is not possible in this particular case.

A sheer line with a constant width sheer, according Fig. 8, is not a problem for the method because the 3-D curves will

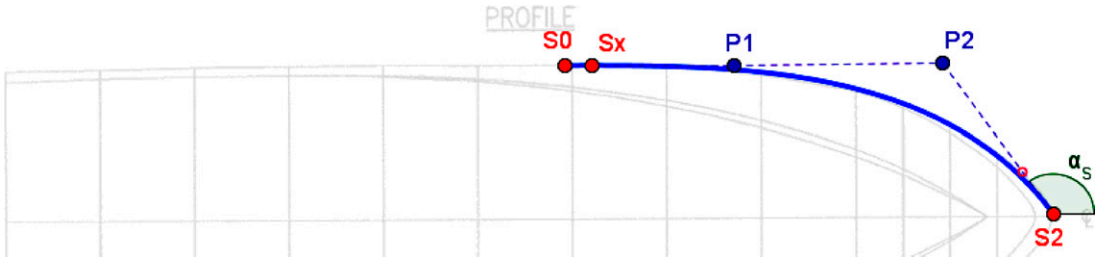

Fig. 8 Sheer line with constant width

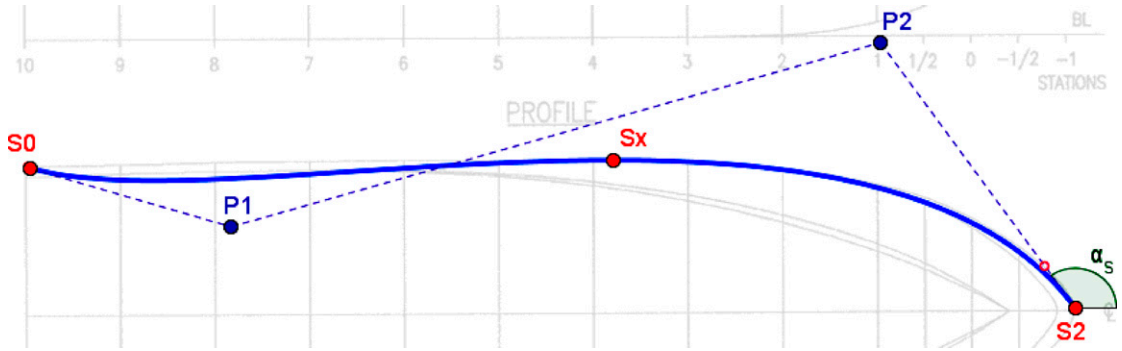

Fig. 9 Nonrealistic sheer

be obtained based on points from the 2-D curves. Therefore, the straight portion, which is not considered, will be modeled using a straight segment between the transom and $\mathbf{S_X}$. Another way to vary the aspect of the curve is to consider different values of k, apart from $k = 1$, in the parameterization of equation (4).

The definition of the sheer line is related to the interior volume distribution above the water, which is linked to the angle α_S; namely, a higher angle increases the useful volume at the fore part of the ship and vice versa. This curve is also related with seakeeping because a reduction in α_S reduces the angle of the bow sections above the water, producing a wider bow. This can produce pounding when advancing in high waves, but it will produce a dry ship in moderate sea states because the water is deflected more pronouncedly than with narrower sections.

3.3. Definition of the sheer line in the lateral view

The sheer line in a profile view and runs from the transom toward the stem in correspondence with its projection in the plan view. Normally, the sheer line will present neither a maximum nor minimum in a planing hull. As a high-speed boat starts onto a plane, it trims up at the bow. With a conventional sheer line, the view over the bow becomes obstructed and, at a critical moment, the view from the helm can be completely blocked. Therefore, the sheer line in the lateral view will start at a given height $\mathbf{S'_0}(0, hs)$ at the transom with a given angle β'_S and will arrive at $\mathbf{S'_2}(Ls, Hs)$ at the stem with a given angle α'_S, as described in Fig. 10. The point $\mathbf{S'_2}$ of the sheer line is equivalent to $\mathbf{K_2}$ of the centerline of Fig. 3.

The restraints of the sheer line in the profile view, $\mathbf{s_L(u)}$, will be $\mathbf{s_L}(0) = \mathbf{S'_0}$, $\mathbf{s_L}(1) = \mathbf{S'_2}$, $s'_L(0) = \mathrm{tg}(\beta'_S)$ and $s'_L(1) = \mathrm{tg}(\alpha'_S)$. These requirements are met with a second-degree B-spline with three control points of the form:

$$s_L(u) = B_0^2 \cdot S_0' + B_0^2 \cdot P_1 + B_2^2 \cdot S_2'$$

The unknown values are the coordinates of $\mathbf{P_1}(XP_1, ZP_1)$ because the curve will contain the end points $\mathbf{S'_0}$ and $\mathbf{S'_2}$. These values will be obtained after imposing the constraints.

The following linear system of equations has to be solved, like in the previous sections:

$$\begin{bmatrix} \mathrm{tg}(\beta_s') & -1 \\ -\mathrm{tg}(\alpha_s') & 1 \end{bmatrix} \cdot \begin{bmatrix} \mathrm{XP_1} \\ \mathrm{ZP_1} \end{bmatrix} = \begin{bmatrix} -\mathrm{hs} \\ \mathrm{Hs} - \mathrm{tg}(\alpha_s') \cdot \mathrm{Ls} \end{bmatrix} \tag{7}$$

In modern designs, the sheer line in the profile view sometimes runs straight. This flat sheer line cannot be modeled with equation (7) because the system of equations has no real solution when $\beta'_S = \alpha'_S$. This can be solved using the properties of the B-spline; aligning the degree + 1 control points produces a straight part of the curve. Therefore, considering $\mathbf{P_1}(XP_1, ZP_1)$ as the middle point of $\mathbf{S'_0}$ and $\mathbf{S'_2}$ produces a valid solution (Fig. 11).

The lateral view of the sheer line is related to the aesthetics and is the most visual line of a ship. The height of $\mathbf{S'_2}$ corresponds to good visibility from the helm station, and this value is also a function of its placement in the general arrangement. If the helm is placed forward, the freeboard Hs can be raised to achieve drier conditions in waves;

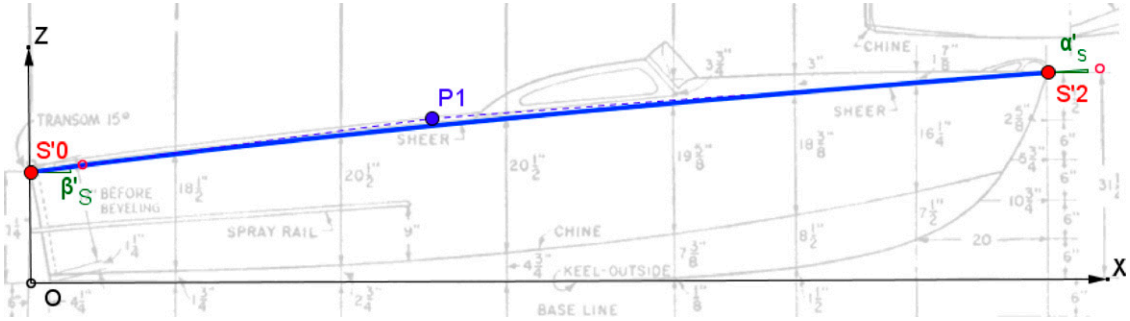

Fig. 10 Sheer definition in the lateral view

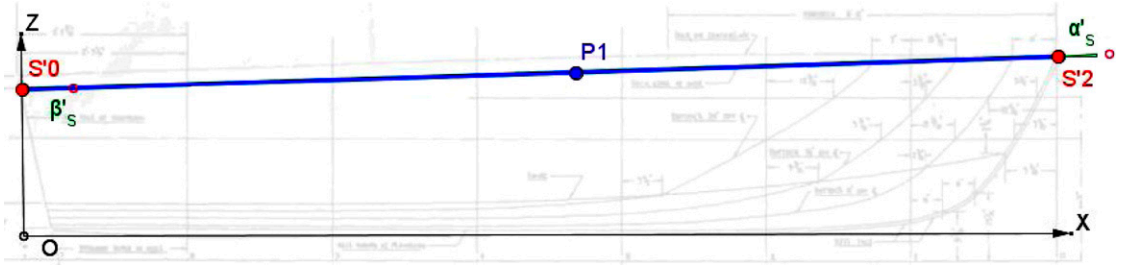

Fig. 11 Flat sheer definition

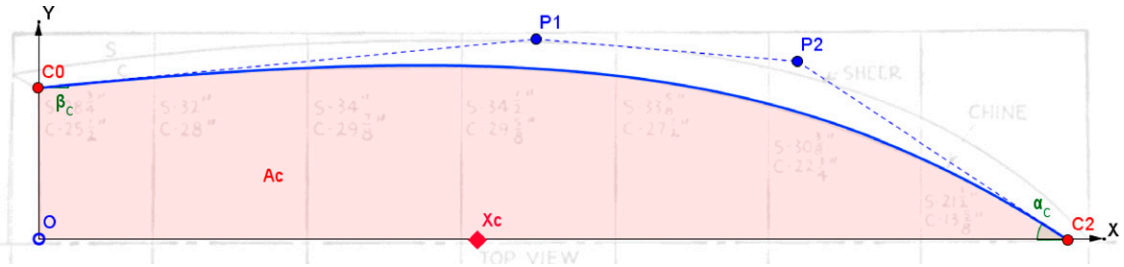

Fig. 12 Chine definition in the plan view

however, a high *Hs* in a small boat tends to be nonaesthetic. A common solution is to reduce the freeboard and raise the helm position.

3.4. Definition of the chine line in the plan view

The chine is the most significant line of a planing hull because it controls the attitude of the craft to go onto a plane. The chine runs from the transom toward the stem (Fig. 12), starting at a point, $\mathbf{C_0}(0, Bc)$, with a given angle, β_c, and arriving at the stem at $\mathbf{C_2}(Lc, 0)$ with an angle, α_c. In this case, the method will impose a confined area (Ac) and the longitudinal position of the center of the enclosed area (Xc). According to Saunders (1957) and Blount and Codega (1992), the area and its centroid have a direct influence on the planing behavior and also on dynamic instabilities of the design. If the hull has a spray rail in the chine (see application examples of Section 4), only the inner part of the chine is considered. The method used to include a spray rail will be explained in Section 3.6 when 3-D curves are created.

Mathematically, these conditions can be imposed with a cubic B-spline with four control points:

$$c_p(u) = B_0^3 \cdot C_0 + B_1^3 \cdot P_1 + B_2^3 \cdot P_2 + B_3^3 \cdot C_2$$

The unknown values are the coordinates of $\mathbf{P_1}(XP_1, YP_1)$ and $\mathbf{P_2}(XP_2, YP_2)$ because the curve will contain the extreme points $\mathbf{C_0}$ and $\mathbf{C_2}$, and $\mathbf{P_1}$ and $\mathbf{P_2}$ will be obtained after imposing the two angle constraints, the enclosed area and its centroid. An important difference between the chine and previously defined lines is that imposing the area and its centroid generates a nonlinear problem.

The angle constraints are introduced as in the previous curves by considering the properties of the control polygon of a B-spline at its ends, which produces the following equations:

$$\mathrm{YP_1} = \mathrm{YC_0} + \mathrm{tg}(\beta_c) \cdot (\mathrm{XP_1}) \tag{8}$$

$$\mathrm{YP_2} = \mathrm{YC_2} + \mathrm{tg}(\alpha_c) \cdot (\mathrm{Lc} - \mathrm{XP_2}) \tag{9}$$

The most difficult part of the problem is the inclusion of the enclosed area and its area centroid into the definition of the problem. Although the area of the closed B-spline can be easily computed with Greens' theorems, in this case, the area is enclosed by the curve and the X-axis. This can be solved by integration in the parametric domain:

$$\mathrm{Ac} = \int \mathrm{dA} = \int_0^{\mathrm{Lc}} Y(t)\mathrm{dX} = \int_0^1 Y(t)X'(t)\mathrm{dt} \tag{10}$$

For this particular case, a cubic B-spline with four control points, $X'(t)$ and $Y(t)$, are cubic polynomials computed with the cubic basis functions of the B-spline and their derivatives (Table 2). The result of the integral of equation (10) can be expressed in matrix form as in equation (11):

$$[X] = \begin{pmatrix} 0 \\ XP_1 \\ XP_2 \\ Lc \end{pmatrix} \quad [Y] = \begin{pmatrix} \mathrm{Bc} \\ \mathrm{YP_1} \\ \mathrm{YP_2} \\ 0 \end{pmatrix} \quad [\Phi] = \begin{pmatrix} \Phi_{00} & \cdots & \Phi_{03} \\ \vdots & \ddots & \vdots \\ \Phi_{30} & \cdots & \Phi_{33} \end{pmatrix} \quad \Phi_{ij} = \int_0^1 B_i^3(t) B_j'^3(t)\mathrm{dt}$$

$$[\Phi] = \begin{bmatrix} -1 & \frac{3}{5} & \frac{3}{10} & \frac{1}{10} \\ -\frac{3}{5} & 0 & \frac{3}{10} & \frac{3}{10} \\ -\frac{3}{10} & -\frac{3}{10} & 0 & \frac{3}{5} \\ -\frac{1}{10} & -\frac{3}{10} & -\frac{3}{5} & 1 \end{bmatrix} \quad Ac = [X]^t \cdot [\Phi] \cdot [Y] \tag{11}$$

The abscissa of the center of gravity of the chine's enclosed area, Xc, can be computed by solving the following integral:

$$Xc = \frac{\int \mathrm{XdA}}{Ac} = \frac{\int_0^{\mathrm{Lc}} X(t)Y(t)\mathrm{dX}}{Ac} = \frac{\int_0^1 X(t)Y(t)X'(t)\mathrm{dt}}{Ac} \tag{12}$$

Like in the previous calculations of the enclosed area, equation (12) can be computed with the cubic basis functions and their derivatives and expressed in matrix form:

$$[X^2] = \begin{pmatrix} 0^2 \\ XP_1^2 \\ XP_2^2 \\ Lc^2 \end{pmatrix} \quad [\hat{X}] = \begin{pmatrix} Lc \cdot XP_2 \\ Lc \cdot XP_1 \\ Lc \cdot 0 \\ XP_2 \cdot XP_1 \\ XP_2 \cdot 0 \\ XP_1 \cdot 0 \end{pmatrix} \quad [\Omega] = \begin{pmatrix} \Omega_{00} & \cdots & \Omega_{03} \\ \vdots & \ddots & \vdots \\ \Omega_{30} & \cdots & \Omega_{33} \end{pmatrix} \quad \Omega_{ij} = \int_0^1 B_i^3(u)B_j^3(u)B_j^{'3}du$$

$$[\Psi] = \begin{pmatrix} \Psi_{32}^0 & \cdots & \Psi_{30}^0 & \Psi_{21}^0 & \Psi_{20}^0 & \Psi_{10}^0 \\ \vdots & \ddots & \vdots & \vdots & \vdots & \vdots \\ \Psi_{32}^4 & \cdots & \Psi_{30}^3 & \Psi_{21}^3 & \Psi_{20}^3 & \Psi_{10}^3 \end{pmatrix} \Psi_{ij}^p = \int_0^1 B_p^3 \left[B_i^3(u)B_j^{'3}(u) + B_j^3(u)B_j^{'3}(u) \right] du \tag{13}$$

$$[\Omega] = \begin{bmatrix} -\frac{1}{3} & \frac{3}{56} & \frac{3}{140} & \frac{1}{168} \\ -\frac{1}{8} & 0 & \frac{9}{280} & \frac{1}{28} \\ -\frac{1}{28} & -\frac{9}{280} & 0 & \frac{1}{8} \\ -\frac{1}{168} & -\frac{3}{140} & -\frac{3}{56} & \frac{1}{3} \end{bmatrix} \quad [\Psi] = \begin{pmatrix} \frac{1}{56} & \frac{1}{70} & \frac{1}{168} & \frac{3}{56} & \frac{1}{28} & \frac{1}{8} \\ \frac{3}{56} & \frac{3}{140} & \frac{1}{280} & \frac{9}{280} & 0 & -\frac{3}{56} \\ \frac{3}{56} & 0 & -\frac{1}{280} & -\frac{9}{280} & -\frac{3}{140} & -\frac{3}{56} \\ -\frac{1}{8} & -\frac{1}{28} & -\frac{1}{168} & -\frac{3}{56} & -\frac{1}{70} & -\frac{1}{56} \end{pmatrix}$$

$$Ac \cdot Xc = [Y]^t \cdot [\Omega] \cdot [X^2] + [Y]^t \cdot [\Psi] \cdot [\hat{X}]$$

Equation (13) is a function of the cross-product of the control point coordinates and their squared and cubic powers. This yields four equations ([8], [9], [11], and [13]) with four unknowns, XP_1, XP_2, YP_1, and YP_2, which form a nonlinear system of equations that must be solved. A direct approach to the solution of such a system can be numerically difficult to obtain because the solution is very sensitive to initial estimates of the solutions. In addition, nonrealistic results can be obtained because of the nonlinearity of equations (11) and (13). Manipulation of the linear conditions of equations (8) and (9) enables further simplifications by substituting YP_1 and YP_2 into equations (11) and (13), yielding:

$$\begin{aligned} &a' \cdot XP_1 + b' \cdot XP_2 + c' \cdot XP_1 \cdot XP_2 + d' = Ac \\ &f' \cdot XP_1^2 + g' \cdot XP_2^2 = h' \cdot XP_1^2 \cdot XP_2 + j'XP_1 \cdot XP_2^2 + \mathrm{k}' \cdot XP_1 \\ &\quad \cdot XP_2 + l' \cdot XP_1 + m' \cdot XP_2 + n' = \\ &= Ac \cdot Lc \end{aligned} \tag{14}$$

where a', b', c',...n' are constants that depend on the initial numerical constraints. The solution of this nonlinear system can be calculated with a Powell hybrid algorithm. This algorithm is a variation of Newton's method, which takes precautions to avoid large step sizes or increasing residuals (More et al. 1980). This method requires the Jacobian of equation (14), which is computed easily in an exact form, and initial estimates of XP_1 and XP_2. Good results are obtained if the estimates of the control points, $\mathbf{P_1}$ and $\mathbf{P_2}$, lie at approximately 50% and 75% of Lc. These assumptions produce realistic solutions in the cases for which they have been tested.

After XP_1 and XP_2 have been obtained, equations (8) and (9) give the remaining coordinates of the control points, and the constrained chine in the plan view is finally defined. If the maximum breadth of the chine is constant, like in the case of prismatic hulls, the solution of equation (14) considering $\beta c = 0$ is mathematically valid. However, this solution is not practical in a similar manner as the sheer curve of Figs. 8 and 9. The reason is the same as that in the case of the sheer line; namely, more than four controls points are needed to reproduce a straight part of a cubic B-spline.

The mathematical model for the chine can be maintained if the constraints are corrected without considering the prismatic part of the chine, as depicted in Fig. 13. In this case, the length of the prismatic body is deducted to $\mathbf{C_2}$ and Xc, and the area of the prismatic part is deduced to Ac; thus, equation (14) is still valid with these assumptions.

Like in the case of the sheer with a constant breadth, the straight part of the curve will be considered to obtain the final 3-D definition of the curve.

The shape of the chine in the plan view is directly related to the planing behavior of the craft. The breadth at the transom is reduced to improve seakeeping because this reduces the wave forces in following seas and increases the dead-rise angle at the transom. As the design speed increases, Xc is moved aft to control the dynamic trim angle and to obtain a finer fore body. Remember that the chine's breadth (Bc) and height (hc)

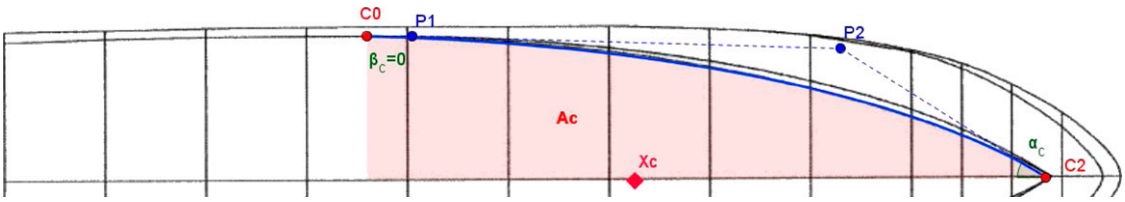

Fig. 13 A chine of constant breadth

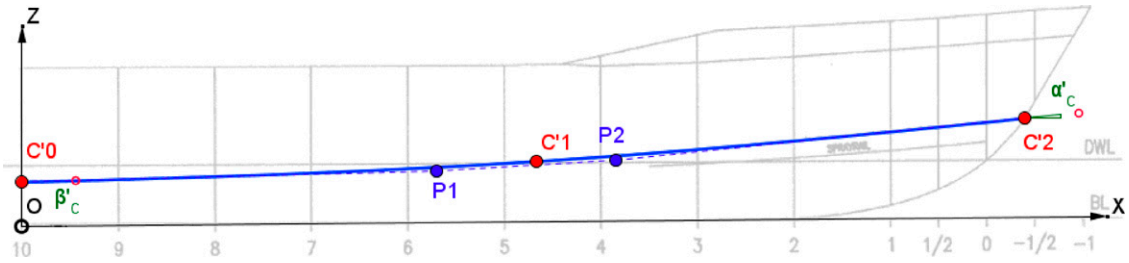

Fig. 14 Definition of the chine in the profile view

at the transom are interrelated with the dead-rise angle at the transom, Ω.

3.5. Definition of the chine line in the lateral view

The chine in the profile view, Fig. 14, runs from the transom at a point $\mathbf{C'_0}(0, hc)$ to $\mathbf{C'_2}(Lc, Hc)$ in the CL. $\mathbf{C'_2}$ is equivalent to $\mathbf{K_1}(Lc, Hc)$ in Fig. 3. The line will start at the transom with a given angle, β'_c, and will arrive at the CL with an angle α'_c, crossing through a point $\mathbf{C'_1}(X_{C1}, X_{C1})$ that is imposed by the designer.

Mathematically, this problem is quite similar to the definition of the CL, although the angle at the aft point of the curve could be nonzero in this case. This curve is defined with a four control point cubic B-spline such as the following:

$$c_L(u) = B_0^3 \cdot C'_0 + B_1^3 \cdot P_1 + B_2^3 \cdot P_2 + B_3^3 \cdot C'_2$$

The unknown values are the coordinates of $\mathbf{P_1}(XP_1, ZP_1)$ and $\mathbf{P_2}(XP_2, ZP_2)$ because the curve will contain the extreme points $\mathbf{C'_0}$ and $\mathbf{C'_2}$. These values will be obtained after imposing the constraints. The first two constraints are related to the tangent angles at the ends of the curve: $c_L'(0) = \mathrm{tg}(\beta'_c)$ and $c'_L(1) = \mathrm{tg}(\alpha'_c)$. The last constraint indicates that the curve interpolates the point $\mathbf{C_1}$ for a certain parameter u^*: $\mathbf{c_L}(u^*) = \mathbf{C_1}$, and u^* is calculated according to equation (4), considering $k = 1$.

Like in the case of the CL, the constraints produce a linear system of equations with the following matrix form:

The solution of this system produces control points $\mathbf{P_1}$ and $\mathbf{P_2}$, and the lateral view of the chine line is completely defined. The lateral projection of the chine largely determines the fore and aft shape of the buttocks, particularly in the after-body. Straight buttocks in the after-body wetted region reduce negative differential pressures in this area and prevent bottom suction and excessive trim by the stern.

The angle β'_c will be nearly zero; therefore, the shape of the chine in the after-body is also controlled by the position of the point $\mathbf{C'_1}$, which can be taken as a reference at the point where the chine intersects the water plane. Therefore, the convexity of the chine, and in turn of the buttocks, is controlled both with a low value of β'_c and with the position of $\mathbf{C'_1}$, which is normally forward of 50% of the ship's waterline length and at the draught's height (Saunders 1957).

A simpler definition of the chine line could be made with a three control-point B-spline, avoiding the intermediate point $\mathbf{C'_1}$, like in the case of the lateral projection of the sheer line. However, the presented curve with four control points provides better control over the curve's shape. The chine's depth in the aft body is determined by the transom dead-rise angle, which is of paramount importance for the hydrodynamic behavior of the design. This point should be slightly below the pretended draft to guarantee that the initial stability of the design will be adequate.

Regarding the chine shape in the fore body, the higher the chine, the better the seakeeping because of the increment of the dead-rise angle in the fore sections. However, this sacrifices the internal volume in this area, and excessive height reduces the buoyancy of the bow.

$$\begin{bmatrix} -\mathrm{tg}(\beta'_c) & 1 & 0 & 0 \\ 0 & 0 & -\mathrm{tg}(\alpha_S) & 1 \\ B_1^3(u^*) & 0 & B_2^3(u^*) & 0 \\ 0 & B_1^3(u^*) & 0 & B_2^3(u^*) \end{bmatrix} \cdot \begin{bmatrix} \mathrm{XP}_1 \\ \mathrm{ZP}_1 \\ \mathrm{XP}_2 \\ \mathrm{ZP}_2 \end{bmatrix} = \begin{bmatrix} h_C \\ \mathrm{Hc} - \mathrm{tg}(\alpha'_C) \cdot \mathrm{Lc} \\ X_{C1} - B_3^3(u^*) \cdot \mathrm{Lc} \\ Z_{C1} - B_0^3(u^*) \cdot \mathrm{hc} - B_3^3(u^*) \cdot \mathrm{Hc} \end{bmatrix} \tag{15}$$

3.6. Generation of the three-dimensional curves

In the preceding sections, the orthographic projections of the main curves of the ship hull have been defined. A direct 3-D approach to the definition of the lines would have been much more difficult and less realistic from the design point of view because these ships are designed based on 2-D sketches of the general arrangement and their associated 2-D curves. Nevertheless, naval architecture software works with a 3-D definition of the hull. Therefore, the next part of the method is to create a 3-D definition of the ship's main lines (upper part of Fig. 2) based on the orthographic projections.

This step is carried out based on a minimum squared fitting of 3-D data points **Qi** obtained from 2-D projections of the curves. These points are obtained by considering the intersection of every pair of curves (CL alone, sheer in the plan and profile views, chine in the plan and profile views) with a set of $np + 1$ abscissas XQi, $i = 0, np$. The corresponding data points for every line, **Qi** (XQi, YQi, ZQi), $i = 0, np$, are obtained in this way.

These abscissas XQi, will lie in the interval $[0, Ls]$ for the center and sheer lines and in $[0, Lc]$ for the chine. It is not necessary to consider them to be uniformly spaced inside the intervals. More data points can be selected in the forward part of the curves, where the curvature is more pronounced than in the aft part, to produce a more accurate fitting. In addition, a different value of np can be used for the chine, sheer, and center lines. Considering a generic cubic curve of the method with four control points and with orthographic projections **c(u)** and **c'(u),** the 3-D points are obtained through the following steps:

$$c(u) = (X(u), Y(u)) = B_0^3 \cdot P_0 + B_1^3 \cdot P_1 + B_2^3 \cdot P_2 + B_3^3 \cdot P_3;$$
$$P_i = (XP_i, YP_i)$$

Obtain the value of u that makes $c(u) = XQ_i$ by solving:

$$XP_0 + u \cdot (-3 \cdot XP_0 + 3 \cdot XP_1) + u^2 \cdot (3 \cdot XP_0 - 6 \cdot XP_1 + 3 \cdot XP_2) + u^3 \cdot (-XP_0 + 3 \cdot XP_1 - 3 \cdot XP_2 + P_3) = XQ_i \quad (16)$$

Substitute u into $Y(u)$ to obtain $YQ_i = Y(u)$.

Repeat the procedure in **c'(u)** = ($X[u]$, $Z[u]$) to obtain ZQ_i, and for $i = 0, np$.

A graphical example is depicted in Fig. 15, where the 3-D data points Qi are obtained for the chine line based on the 2-D curves that define this line.

Equation (16) is obtained by expanding the equation of a cubic B-spline with four control points by considering the basis functions of Table 2. In the case of the CL, there is only its profile view. If a rocker value is used (Fig. 6), the procedure must be repeated separately for the two curves that form the CL. If this line does not present a rocker (Fig. 3), the points on the straight segment between the origin and the point $\mathbf{K_0}$ are easy to obtain.

In the case of the sheer line in the lateral view (Fig. 10), the curve is modeled with just three control points instead of four. This produces a simplification in the procedure, and equation (16) is substituted by the following equation:

$$XP_0 + u \cdot (-2 \cdot XP_0 + 2 \cdot XP_1) + u^2 \cdot (XP_0 - 2 \cdot XP_1 + XP_2) = XQ_i \quad (17)$$

After $np + 1$ data points $\mathbf{Q_i}$, have been obtained, the fitting begins. A large number of data points does not suggest the use of an interpolating B-spline. Instead, an approximating curve is needed. For every curve of index "d," the B-spline

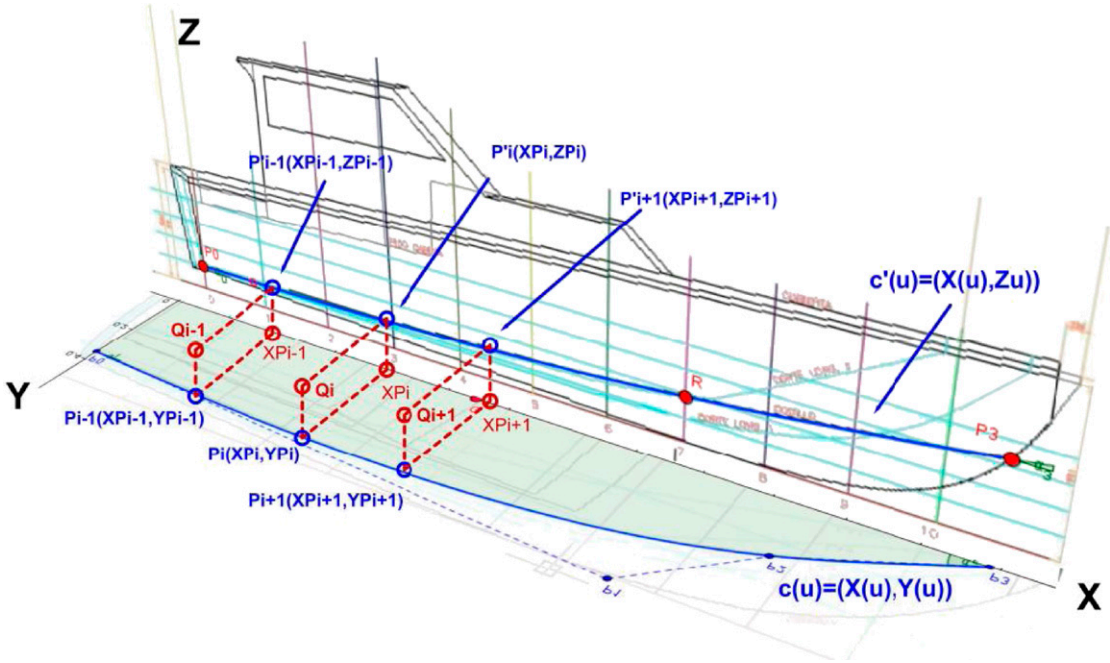

Fig. 15 Obtaining the three-dimensional points Q_i

$\mathbf{c_d(u)}$ will not cross through the data points exactly, but it will instead pass close enough to the points to capture the inherent shape. This is a least squares (LS) approximation (Piegl & Tiller 1997).

In this problem, $np + 1$ data points, $\mathbf{Q_0}, \ldots \mathbf{Q_{np}}$, will be approximated by a p^{th} degree B-spline with $N + 1$ control points, $\mathbf{P_0}, \ldots \mathbf{P_N}$, $N < np$, that are unknown and are obtained as the final result of the calculations.

The general LS problem is described by the following overdetermined set of $np + 1$ equations with $N + 1$ unknown variables:

$$\begin{array}{c} B_0^p(t_0)\cdot P_0 + B_1^p(t_0)\cdot P_1 + \ldots + B_N^p(t_0)\cdot P_N = Q_0 \\ B_0^p(t_1)\cdot P_0 + B_1^p(t_1)\cdot P_1 + \ldots + B_N^p(t_1)\cdot P_N = Q_1 \\ \vdots \qquad\qquad \vdots \qquad\qquad \vdots \qquad\qquad \vdots \\ B_0^p(t_{np})\cdot P_0 + B_1^p(t_{np})\cdot P_1 + \ldots + B_N^p(t_{np})\cdot P_N = Q_{np} \end{array} \tag{18}$$

where B_i^p corresponds to the i^{th} basis function of a p^{th} degree B-spline, which was calculated using de Boor's algorithm of equation (2) by considering a uniform knot vector. t_j $(j = 0, n)$ represents the parameters associated with the data points. The following matrix expression is convenient for solving this problem:

$$\begin{bmatrix} B_0^p(t_0) & B_1^p(t_0) & \ldots & B_N^p(t_0) \\ B_0^p(t_1) & B_1^p(t_1) & \ldots & B_N^p(t_1) \\ \vdots & \vdots & \vdots & \vdots \\ B_0^p(t_{np}) & B_1^p(t_{np}) & \ldots & B_N^p(t_{np}) \end{bmatrix} \cdot \begin{bmatrix} P_0 \\ P_1 \\ \vdots \\ P_N \end{bmatrix} = \begin{bmatrix} Q_0 \\ Q_1 \\ \vdots \\ Q_{np} \end{bmatrix}; [\mathrm{M}]\cdot[P] = [Q] \Rightarrow [\mathrm{M}]^{\mathrm{T}}\cdot[\mathrm{M}]\cdot[P] = [\mathrm{M}]^{\mathrm{T}}\cdot[Q] \tag{19}$$

This system of equations is solved by multiplying both sides of equation (19) by $[\mathrm{M}]^{\mathrm{T}}$, which creates a determined $(N + 1)$ by $(N + 1)$ linear system. This type of system can be poorly conditioned, especially if a large number of control points is used. A conventional technique should not be used to solve this ill-conditioned system. Instead, a single-value decomposition of $[\mathrm{M}]^{\mathrm{T}}\cdot[\mathrm{M}]$ and a later back-substitution process are performed. The solutions of this system are the control points of the best-fitting B-spline.

Approaching this problem with a standard parameterization such as centripetal or chord length, is correct but does not take into consideration the effect of the distance of the data points from the B-spline. In this method, a parameterization based on a minimum distance is adopted. The process is iterative and is described by the following three steps:

1. The method starts with a centripetal parameterization of the $\mathbf{Q_i}$ points, and system (equation [18]) is solved. This produces a starting curve of the iterative process, which is only used for the first loop.
2. For each $\mathbf{Q_i}$, the minimum distance to the B-spline is calculated. This is done by dividing the B-spline $\mathbf{c_d(u)}$ into Bézier curves $\mathbf{b_j(u_L)}$ $(j = 1, N - p)$ of the p^{th} degree and computing the minimum distance to the corresponding Bézier piece, leading to a solution of equation (20).

$$\left(Q_i - b_j(u_L)\right)\cdot\left(b_j'(u_L)\right) = 0 \tag{20}$$

This equation is solved in the local domain of the Bézier curves. The equation is a polynomial, $u_L \in [0,1]$; therefore, specific algorithms for this type of equation can be used. These algorithms do not require an initial guess, which would be required if a Newtonian method were used in the B-spline domain. The current method uses a Jenkins-Traub three-stage algorithm (Jenkins & Traub 1970). The valid solution will be a noncomplex solution of $u_L \in [0,1]$.

After the solution has been found, the local u_L for the Bézier domain is easily converted into its global value, t_i, in the B-spline domain. This t_i value is the parameter associated with the point $\mathbf{Q_i}$ when solving system equation (19).

3. After obtaining the t_i $(i = 1,np)$ values, the distance $d_i = (\mathbf{Q_i} - \mathbf{c_d}[t_i])$ is computed, which is the Euclidean distance between $\mathbf{Q_i}$ and the B-spline. This distance is used to check the shape requirement. If the maximum distance d_i $(i = 1, n)$, is above a given tolerance, steps 2 and 3 are repeated until an acceptable maximum distance is achieved. The quality of the obtained curve is measured using the tolerance constraint, and the shape of the B-spline is amended using parameterization (equation [20]).

If the tolerance is not obtained in fewer than 50 iterations, the number of control points $N + 1$ has to be increased. The increment of the degree p in this procedure can also reduce the maximum distance. However, increasing the number of control points has a more substantial effect, and a higher degree raises the complexity and the computational time. A block diagram of the fitting process follows.

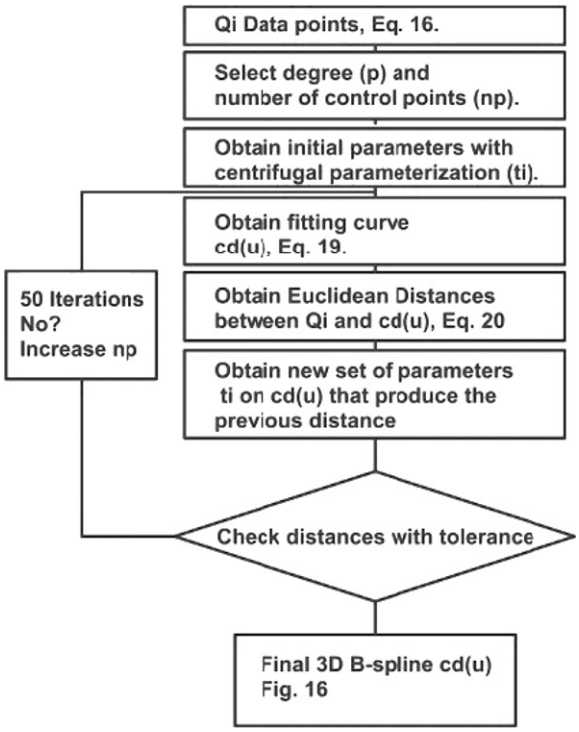

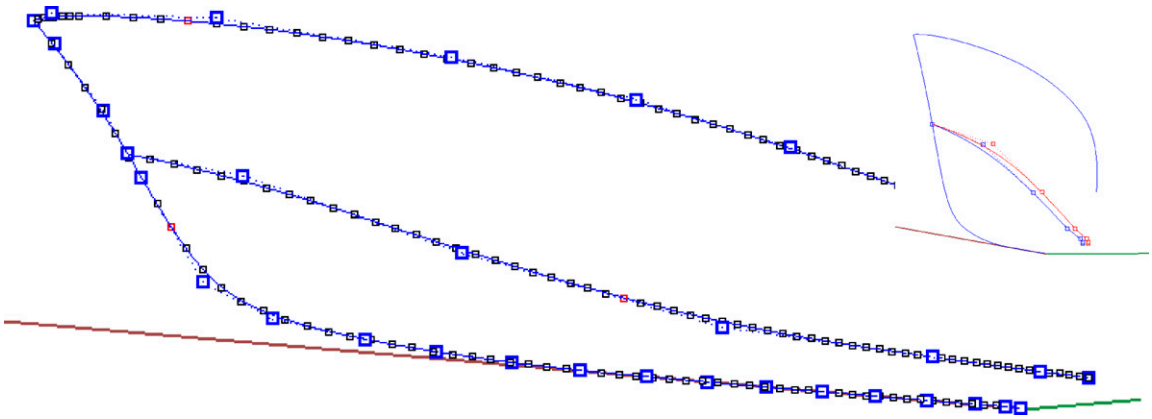

Fig. 16 Example of three-dimensional curves and how a spray rail is created

When the fitting is finished for all the curves, a set of three B-splines is obtained. Figure 16 presents an example of the described fitting. This particular example shows a cubic B-spline fitting of a ship of maximum dimensions $Ls = 16.94$ m, $Bx = 2.42$ m, and $Hs = 3.27$ m. The sheer line has been modeled with 10 control points with a maximum tolerance of 0.008 m and a medium tolerance of 0.002 m. The chine has been modeled with seven control points, and the tolerances are maximum = 0.007 m and median = 0.004 m. The CL has 19 control points and tolerances of maximum = 0.009 m and median = 0.001 m.

The curves need more control points to achieve a given tolerance when they present a more pronounced curvature. For example, the CL has a more pronounced curvature because of its forefoot and the sheer line as a result of its forward part. The presented example is representative of the number of control points and the tolerances that can be achieved with the proposed method.

The foremost end of the 3-D chine curve will be close to the CL, below the tolerance, but not exactly on the CL because of the fit of the CL points. This is corrected by perpendicularly projecting this point over the B-spline that represents the CL. A spray rail can be obtained in the chine by adding the width of the rail to the Y coordinate of the control points of the chine line (Fig. 16, right) with the exception of the control point placed on the CL. This simple approach produces realistic results.

3.7. Definition of the stations

The next step is the creation of the stations where the hull surfaces will rest. These curves will be formed from two pieces, one between the CL and the chine and the second one between the chine and the sheer line, because of the topology of the hull. If a spray rail had been created, like in Fig. 16 (right), the station would contain a straight segment within the inner and the outer chine lines. Therefore, the first step is to define the ends of the pieces for every station by calculating the intersection points of the 3-D curves with different planes Xi, $i = 1, q$, perpendicular to the X-axis and inside the interval $[0, Ls]$.

The intersection points are obtained numerically by subdividing the B-spline curves into Bézier pieces and then proceeding in a similar way as in Section 3.6 to obtain data points for the minimum squares fitting.

The stations of a planing hull can be convex, concave, or straight. In addition, they can change their type along the length of the ship. For example, the part of the station under the chine is convex most of the time (Fig. 17, left), whereas the upper part between the chine and the sheer can be a concave curve (Fig. 17, right), particularly if the fore part of the ship is designed to expel

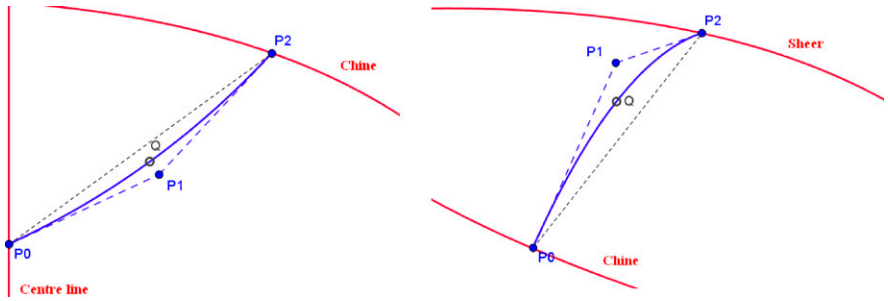

Fig. 17 Definition of the stations; convex or concave curves

the water when advancing in bow waves. Thus, the convex/concave aspect of the curve must be controlled.

A set of q stations will be defined. For every piece of a station below and above the chine, the method uses a second-degree B-spline with three control points:

$$c_d(u) = B_0^2 \cdot P_0 + B_1^2 \cdot P_1 + B_2^2 \cdot P_2; \quad d = 0, q-1$$

The ends of the curves $\mathbf{P_0}(YP_0, ZP_0)$ and $\mathbf{P_2}(YP_2, ZP_2)$ will be placed in the 3-D curves and are calculated as described previously, whereas the second control point, $\mathbf{P_1}$, will be calculated to obtain a given concavity/convexity.

The amount of concavity is set by interpolating a given point, **Q**. In the proposed method, this point is defined by a given distance to the segment $\mathbf{P_0P_2}$ and by a given position along $\mathbf{P_0P_2}$. The distance is set relative to the length of the segment $\mathbf{P_0P_2}$ and can be positive or negative, i.e., 5% of $\mathbf{P_0P_2}$.

Mathematically, the B-spline $\mathbf{s_i(u)}$, interpolates **Q** at $u = 0.5$. This has the advantage of producing a tangent line at **Q** that is parallel to $\mathbf{P_0P_2}$ because of the properties of second-degree B-spline curves. In this manner, the deflection of the curve from the segment $\mathbf{P_0P_2}$ is controlled. Moving **Q** along the length $\mathbf{P_0P_2}$ helps to round the ends of the curve, which is helpful near the CL in the fore part (forefoot) or close to the sheer line in the case of convex stations. The coordinates of $\mathbf{P_1}$ are calculated as follows:

$$\mathrm{P1} = \left(\mathrm{Xi}, 2 \cdot \mathrm{Y}_Q - \frac{\mathrm{YP}_0 + \mathrm{YP}_2}{2}, 2 \cdot Z_Q - \frac{\mathrm{ZP}_0 + \mathrm{ZP}_2}{2}\right) \quad (21)$$

Realistic results can be obtained by placing the projection of **Q** over $\mathbf{P_0P_2}$ at the midpoint of this segment and by using a deflection of −5% to +5%, depending on the design characteristics. Examples of the stations that can be obtained with the presented method are depicted in Fig. 18. In this example, **Q** lies in the middle of $\mathbf{P_0P_2}$ for every station and maintains a distance of 3% $\mathbf{P_0P_2}$ both below and above the chine.

The next example (Fig. 19) uses the same 3-D curves as the prior example, but the position of **Q** is different for the bow sections. The forefoot of the curves below the chine is a bit more rounded; **Q** lies at 30% of $\mathbf{P_0P_2}$ at the forward stations and the deflection is maintained at 3%. Over the chine, **Q** lies at approximately 60% of $\mathbf{P_0P_2}$ with a deflection of approximately −5% for the fore sections.

After the stations have been calculated, the resulting wire model of the ship hull enables hydrostatic and stability calculations to be made with reasonable precision.

The distribution of **Q** along the ship's length is a good indicator of the fairing of the hull. Thus, if the position of **Q** is plotted for the different stations, the resulting curve should be soft and without

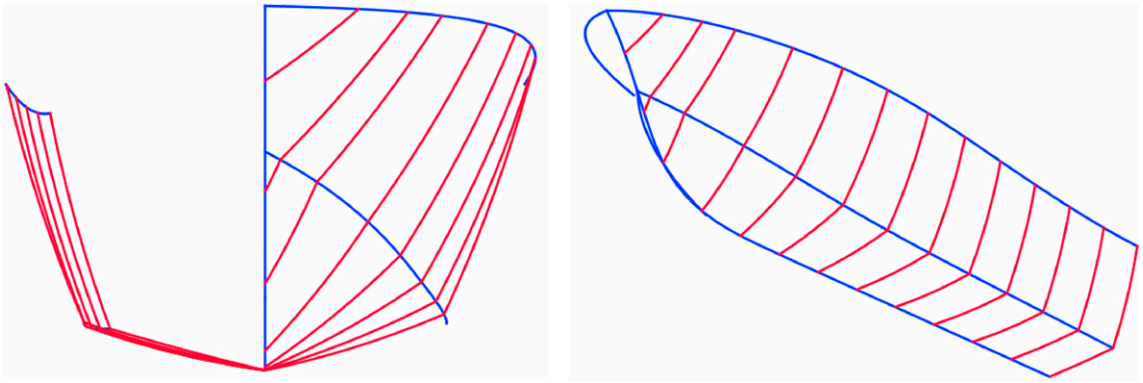

Fig. 18 Example of a ship with convex stations over the chine

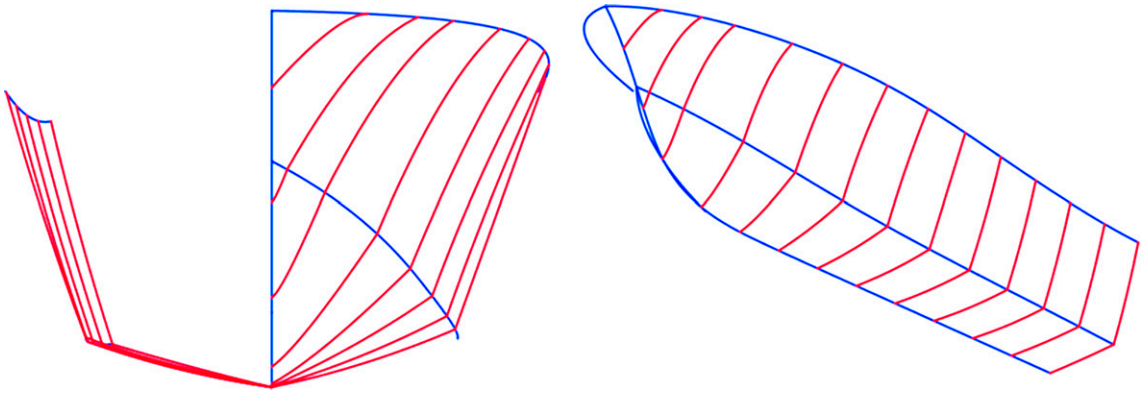

Fig. 19 Example of a ship with concave stations over the chine

bumps or hollows. This will produce faired hull surfaces that will rest on the calculated stations, as explained in the next section.

3.8. Lofting surface of the stations

The last step of the method is the definition of B-spline surfaces that lean on the stations previously defined, one surface between the chine and the CLs and a second one between the chine and the sheer lines. If a spray rail exists, this will produce a third surface between the inner and outer chine lines.

The generalization from curves to surfaces is not difficult as a result of the properties of B-splines, and a lofting surface of the station pieces can easily be defined. Lofting (or skinning) is one of the most widely used tools for interactive shape description in CAD with different peculiarities, i.e., Woodward (1988). The transition from spline curves to spline surfaces is achieved by turning the control polygon into a control net of control points $\mathbf{W_{ij}}(X_{ij}, Y_{ij}, Z_{ij})$ using the same B-spline basis for the two parameters u and v as well as using two different lists of knots: $\{u_{-1},\ldots,u_{N+n}\}$ and $\{v_{-1},\ldots,v_{M+m}\}$.

The lofting process of a set of q B-splines (station pieces) with the same degree and list of knots is as follows: find a B-spline surface $\mathbf{S}$ with degree n by m and $(N + 1)$ by $(M + 1)$ control points and a list of knots $\{u_{-1},\ldots,u_{N+n}\}$ and $\{v_{-1},\ldots,v_{M+m}\}$ according to equation (22) that interpolates q different B-splines $\mathbf{c_d}$ $(d = 0,\ldots, q-1)$ of n^{th} degree with $N + 1$ control points and a list of knots $\{u_{-1},\ldots,u_{N+n}\}$ with the form of equation (23).

$$S(u,v) = \sum_{i=0}^{N}\sum_{j=0}^{M} \mathbf{W_{ij}} \cdot B_i^n(u) \cdot B_i^m(v) \tag{22}$$

$$\mathbf{c_d}(u) = \sum_{i=0}^{N} \mathbf{V_{id}} \cdot B_i^n(u) \qquad (d = 0,\ldots,q-1) \tag{23}$$

Note that $\mathbf{V_{id}}$ are the control points of the different stations obtained in Section 3.7 and expressed in matrix form. Values for N, M, and q depend on user preferences regarding the definition of the surface. The interpolation can be written as:

$$S(u,v_d) = \sum_{i=0}^{N}\left(\sum_{j=0}^{M} \mathbf{W_{ij}} \cdot B_j^m(v_d)\right) \cdot B_i^n(u) = \sum_{i=0}^{N} \mathbf{V_{id}} \cdot B_i^n(u) = \mathbf{c_d}(u) \qquad (d = 0,\ldots,q-1) \tag{24}$$

This group of equations has to be solved for a set of values of parameter v_d $(d = 0,\ldots, q-1)$, termed the choice of the parameterization. The centripetal parameterization produces good results for ship hulls. By identifying equal coefficients for every row of equation (24), $i = 0,..N$, the following linear system is obtained:

$$\sum_{j=0}^{M} \mathbf{W_{ij}} \cdot B_j^m(v_d) = \mathbf{V_{id}} \qquad (d = 0,\ldots q-1)$$

To obtain a unique solution for this system, $M + 1$ must equal q, where q is the number of stations that defines the surface. The $(M + 1)$ by $(N + 1)$ solutions are the control points $\mathbf{W_{ij}}$ of the lofting surface of equation (22) containing the stations.

3.9. Some comments on the performance effect of the parameters

The forefoot contour is related to the directional stability in smooth and cross seas; cross seas tend to throw the bow around. A deep forefoot with a high value of α_K produces a narrow bow and increases the dead-rise angle of the bow sections, improving performance at low speeds.

A clipper bow that has an "S" shape above the waterline can be achieved by reducing α_K. This will produce convex sections on the bow that will deflect the water, producing a drier ship in head seas.

The use of a rocker is common in semidisplacement hulls designed to go more through the water than planing on top. This is because the aft buttocks are not straight. The use of a hook is not common today, and a better effect can be obtained with the use of adjustable trim tabs.

The definition of the sheer line is related to the interior volume distribution above the water, which is linked to the angle α_S; namely, a higher angle increases the useful volume at the fore part of the ship and vice versa. This curve is also related with seakeeping because a reduction in α_S reduces the angle of the bow sections above the water, producing a wider bow. This can produce pounding when advancing in high waves, but it will produce a dry ship in moderate sea states

Table 3 Parameters of the examples

Name	Example 1	Example 2
Ls	124.0	25.6
L0	66.5	14.8
Lx	62.8	14.8
Lc	114.4	23.4
Xc	49.3	9.9
X_{C1}	55.4	10.2
Bs	11.1	4.1
Bx	13.7	4.8
Bc	10.2	4.0
Sp	1.2	0.3
Hs	16.3	4.5
Hc	11.2	2.9
hr	0.0	0.0
hs	12.8	3.3
hc	3.3	1.5
Z_{C1}	4.6	1.6
α_K	29	35
α_S	129	98
β's	2	4
α'_S	1	0
α_C	23	49
β_C	1	2
α'_C	8	7
β'_C	0	1
$2 \cdot Ac$	2049	153

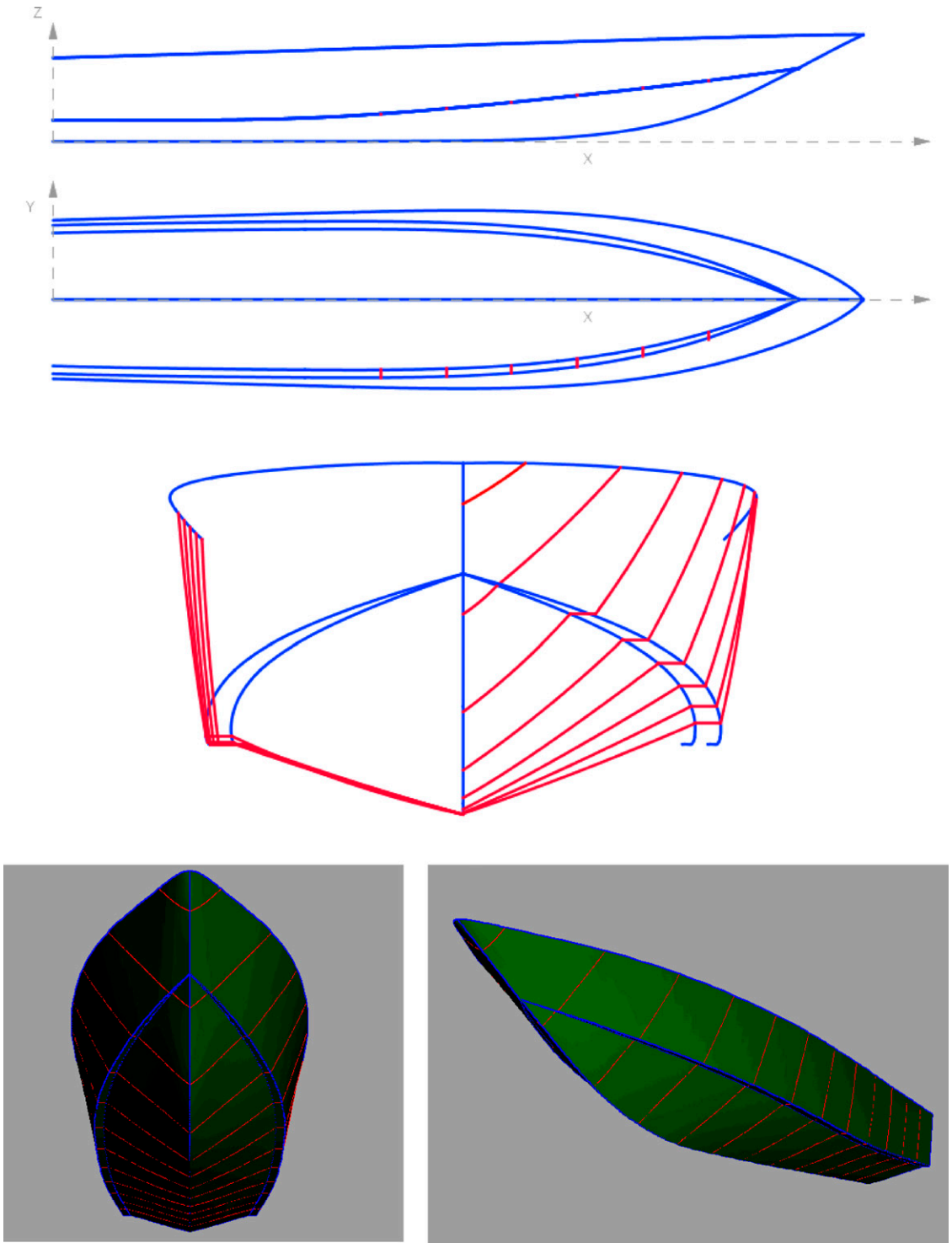

Fig. 20 Example 1: a motor yacht

because the water is deflected more pronouncedly than with narrower sections.

The lateral view of the sheer line is related to the aesthetics and is the most visual line of a ship. The height of $\mathbf{S'_2}$ corresponds to good visibility from the helm station, and this value is also a function of its placement in the general arrangement. If the helm is placed forward, the freeboard *Hs* can be raised to achieve drier conditions in waves; a high freeboard increases wind resistance, noticeable at very high Froude numbers.

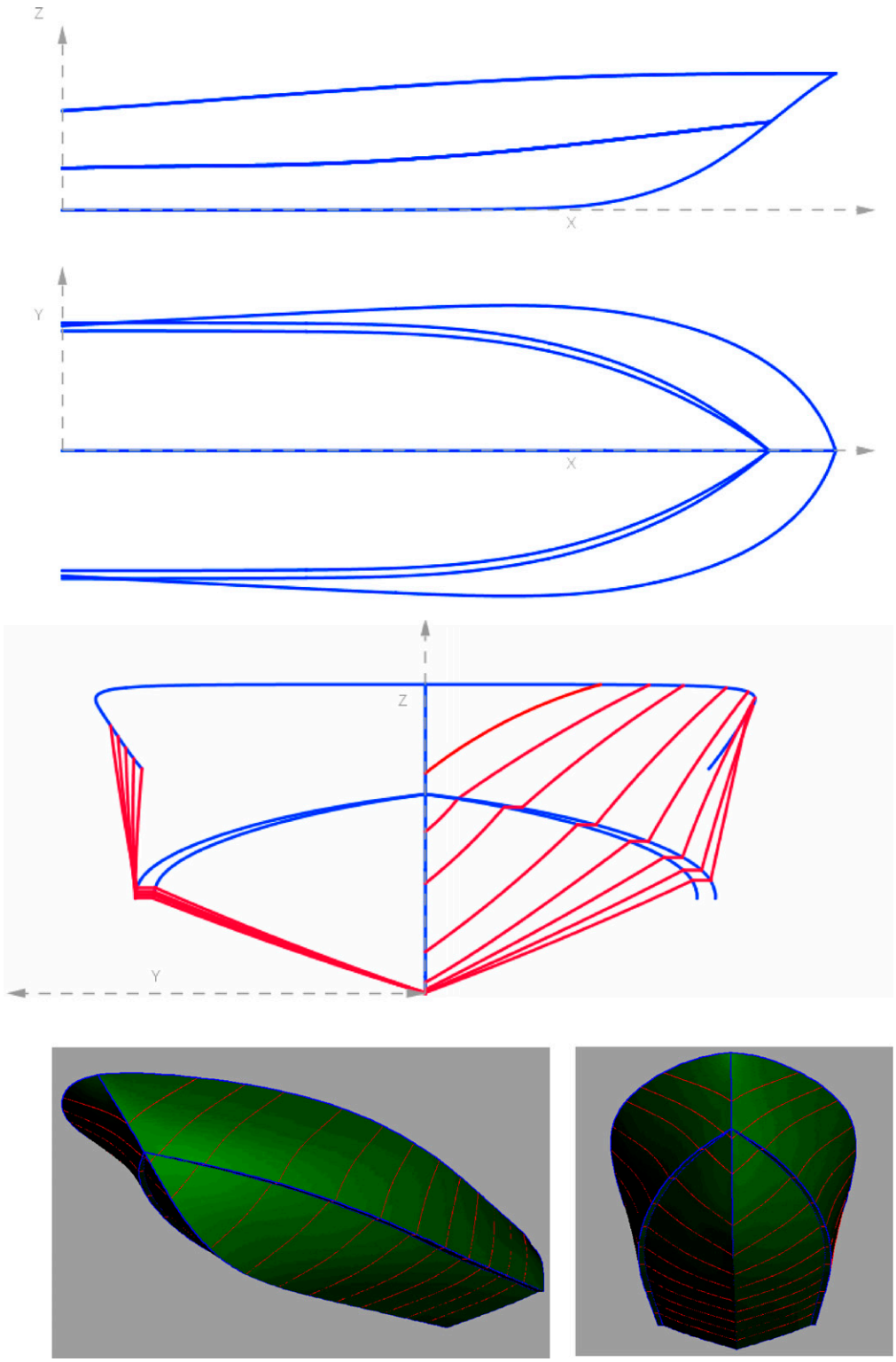

Fig. 21 Example 2: a recreational craft

The shape of the chine in the plan view is directly related to the planing behavior of the craft and directly related with the bottom loading coefficients (Blount & Codega 1992). The breadth at the transom is reduced to improve seakeeping because this reduces the wave forces in following seas and increases the dead-rise angle at the transom. As the design speed increases, *Xc* is moved aft to control the dynamic trim angle and to obtain a finer fore body.

The chine's depth *hc* in the aft body is determined by the transom dead-rise angle, which is of paramount importance for the hydrodynamic behavior of the design. This point should be slightly below the pretended draft to guarantee that the initial stability of the design will be adequate. Regarding the chine shape in the fore body, the higher the chine, the better the seakeeping because of the increment of the dead-rise angle in the fore sections. However, this sacrifices the internal volume in this area, and excessive height reduces the buoyancy of the bow.

4. Application examples

This section presents two applications of the method, which can be constructed with the parameters in Table 3. The first example shows a 126-foot (37.8 m) fast motor yacht. Notice the convex forward sections (Fig. 20) and the absence of warp at the bottom. Dead-rise is 18° in the transom, and the keel is flat for an undisturbed center-jet inlet and for lift.

The second example in Fig. 21 shows a 26-foot (7.9 m) recreational craft. The dead-rise is 20° in the transom, so it can be considered a deep V hull. Notice the concave sections at the bow over the chine that produce a dryer ship and the reverse sheer in the aft, whereas a wide aft planing surface is maintained. Both hulls have a spray rail.

For the first example, and according to Section 3.7, the maximum deflection of the stations varies linearly between 1% and 2% for the aft and fore sections, and the deflection is placed in the middle of the segment $\mathbf{P_0P_2}$ (u = 0.5). Example 2 presents concave sections in the bow area over the chine. For this example, the maximum deflection is between 1% and 2% with negative values for the concave stations and like in the previous case, the variation is linear along the ship's length.

The projections of the center, sheer, and chine lines calculated according to the method are shown at the top of Figs. 20 and 21, whereas a 10-station front view is depicted in the middle of the figures, according to Section 3.7. The 3-D lines were calculated by considering 80 points for every 3-D curve and adjusting those points with a B-spline curve to obtain a maximum tolerance of 0.0l-feet, following Section 3.6. The lower part of the figures shows rendered views of the lofting surfaces of Section 3.8 that define the ship hulls.

5. Conclusions

This article has presented a practical method for defining the hull of a planing hull based on geometric parameters that are characteristic of this type of ship hull. This constrained definition enables rapid changes in the design procedure and prevents unnecessary manual work from being done because a valid hull form can be automatically generated and geometrically constrained to the design parameters.

The ability to change the characteristics of the ship hull by modifying numerical parameters rather than by manipulating tens of surface control points is beneficial and was the motivation behind this research. The method presented here is a good compromise when creating a hull that can be manually modified at a later time to add complex features like spray strakes or appendages because these characteristics are difficult to define by parameters.

The method is based on projections of the significant lines of the hull including the center, sheer, and chine lines. These lines were defined based on geometrical constraints without the use of templates. The transformation of a template in a planing hull can change important parameters of this type of ship such as the dead-rise angle. This can alter the performance compared with the original template.

The method presented here can reproduce specific features of planing hulls such as a straight sheer or a CL with some rocker. The method can also include the enclosed area and its centroid into the chine definition, which are important parameters related to the operation of the ship.

After these 2-D lines have been defined, corresponding 3-D curves were defined using a least squared fitting that considered a distance tolerance in its parameterization.

The stations of the design can include a certain amount of convexity/concavity that is different based on the type of design (e.g., fishing vessels, recreational crafts).

The number of longitudinal and transverse control points on the final surfaces can be defined such that the definition of the surface can be increased and then manually modified in later stages to include appendages or other design requirements that may be difficult to include in the initial definition of a constrained design procedure. The final result is a set of two B-spline surfaces that can be easily exported to specialized computer programs for further stages of the design process.

Acknowledgments

We thank Ing. Francesco Volpe from Genoa University for his support in CAD definitions.

References

Ayob, A. F., Ray, T., and Smith, W. F. 2009 An optimization framework for the design of planing craft, *Proceedings*, International Conference on Computer Applications in Shipbuilding, ICCAS, September 1–3, Shanghai, China, p. 1028–1057.

Ayob, A. F., Ray, T., and Smith, W. F. 2010 Hydrodynamic design optimization of a hard chine planing craft for coastal surveillance, *Proceedings*, International Maritime Conference Pacific, January 27–29, Sydney, Australia, pp. 73–82.

Blount, D. L., and Codega L. T. 1992 Dynamic stability of planing boats, *Marine Technology*, **29**, 1, 4–12.

Bole, M. 2002 A hull surface generation technique based on form topology and geometric constraint approach. PhD thesis, University of Strathclyde, Strathclyde, UK.

Calkins, D. E., Schachter, R. D., and Oliveira, L. T. 2001 An automated computational method for planing hull form definition in concept design, *Ocean Engineering*, **28**, 3, 297–327.

Clement, E., and Blount, D. 1963 Resistance tests of a systematic series of planing hulls, Transactions of the SNAME, **71**, 491–579.

Creutz, G., and Schubert, C. 1978 Interactive curve creation from form parameters by means of B-splines, *Schiffstechnik*, **25**, 121–145.

Farin, G. 2001 Curves and Surfaces for CAGD. Morgan Kaufmann, Elsevier, San Francisco, CA.

Jenkins, A., and Traub, J. 1970 A three-stage variable-shift iteration for polynomial zeros and its relation to generalized rayleigh iteration, *Numerische Mathematik*, **14**, 3, 252–263.

Keane, A. J. 1988 A computer based method for hull form concept design: applications to stability analyses, *Transactions RINA*, **130**, 61–75.

KIM, H. C. 2004 Parametric design of ship hull forms with a complex multiple domain surface topology. PhD thesis, Tech. Universität Berlin, Berlin, Germany.

KUIPER, G. 1970 Preliminary design of ship lines by mathematical methods, JOURNAL OF SHIP RESEARCH, **14**, 52–66.

MANCUSO, A. 2006 Parametric design of sailing hull shapes, *Ocean Engineering*, **33**, 234–246.

MORE, J., BURTON, G., AND HILLSTROM, K. 1980 User guide for MINPACK-1, Argonne National Labs Report ANL-80-74, Argonne, IL.

NAM, J. H., AND PARSONS, M. 2006 A parametric approach for initial hull form modelling using NURBS representation, Journal of Ship Production, **16**, 2, 76–89.

PÉREZ F., CLEMENTE J. A., SUÁREZ J. A., AND GONZÁLEZ J. M. 2008 Parametric generation, modeling, and fairing of simple hull lines with the use of non uniform rational B-spline surfaces, Journal of Ship Research, **52**, 1, 1–15.

PIEGL, L. A., AND TILLER, W. 1997 The NURBS Book. Springer, New York, NY, pp. 410–413.

REED, A. M., AND NOWACKI, H. 1974 Interactive creation of fair ship lines, *Journal of Ship Research*, **18**, 96–112.

SAUNDERS, H. E. 1957 Hydrodynamics in Ship Design, sec. 77. Society of Naval Architects and Marine Engineers, New York, NY, 400 pp.

SAVITSKY, D. 1964 Hydrodynamic design of planing hulls, *Marine Technology*, **1**, 1, 1964.

SAVITSKY, D., AND BROWN, W. 1976 Procedures for hydrodynamic evaluation of planing hulls in smooth and rough water, *Marine Technology*, **13**, 381–400.

WOODWARD, C. D. 1988 Skinning techniques for interactive B spline surface interpolation, *Computer Aided Design*, **20**, 441–451.

YILMATZ, H. AND KUKNER, P. 1999 Evaluation of cross curves of fishing vessels at the preliminary design stage, *Ocean Engineering*, **26**, 979–990.